This article has been accepted for publication in IEEE Access. This is the author's version which has not been fully edited and content may change prior to final publication. Citation information: DOI 10.1109/ACCESS.2024.3392734

Date of publication xxxx 00, 0000, date of current version xxxx 00, 0000.

Digital Object Identifier 10.1109/ACCESS.2023.Doi Number

Design of a Novel PID Controller Based on Machine Learning Algorithm for a Micro-Thermoelectric Cooler of the Polymerase Chain Reaction Device

Yılmaz Seryar ARIKUŞU [1] (Student Member,IEEE), Nevra BAYHAN [2]

[1] Department of Electrical Engineering, Manisa Celal Bayar University, Manisa, Turkey
[2] Department of Electrical and Electronics Engineering, Istanbul University-Cerrahpaşa, Istanbul, Turkey

Corresponding author: Nevra BAYHAN (e-mail: nevra@iuc.edu.tr)

ABSTRACT The combined use of Extreme Gradient Boosting (XGBoost) algorithm, one of the machine learning (ML) methods, and a generalization of Hermite-Biehler theorem to obtain a novel PID controller that will ensure robustly stable and optimized operation of a micro thermoelectric cooler (Micro-TEC), which is the main part of a Polymerase chain reaction (PCR) device, is a unique approach of our study compared to previous studies. Therefore, we first established a mathematical model of the micro-TEC by making real-time measurements and then, a new data set was created to find the optimum parameter values of PID controller, and finally, XGBoost Hyperparameters with GridSearchCV was used for the first time to predict PID controller parameters. The XGBoost algorithm achieved 97% training success and 91% test success in estimating the parameters of the PID controller. Moreover, the novel controller developed using the XGBoost algorithm in this study has an impressive speed of 3 seconds. Additionally, our proposed method was compared with various metaheuristic optimization algorithms in terms of error percentage. The error percentages of XGBoost, the equilibrium optimization, the particle swarm optimization and the artificial bee colony optimization algorithms were found to be 0.4%, 1.1%, 3.7% and 11.1%, respectively. It is observed the settling times of micro-TEC with ML-PID controller for all five PCR cycles are 4.86, 44, 83.4, 123 and 162.5 seconds, respectively, and the overshoot values are below 5%. The proposed method gave the smallest settling time, error and overshoot percentages compared to these metaheuristic optimization algorithms.

INDEX TERMS XGBoost algorithm, GridSearchCV, Thermoelectric cooler, Machine learning

I. INTRODUCTION

One of the most important and widely applied technologies in medical and biological research is the polymerase chain reaction (PCR), which was developed by Mullis et.al [1]. Polymerase chain reaction (PCR) device, which has become increasingly important during the Covid 19 pandemic, is used to detect genes using appropriate enzymes under cycle temperature values [2], [3]. Thermocyclers, commonly known as polymerase chain reaction equipment, are laboratory equipment that enable quick replication of tremendously small amounts of DNA in a short period of time [4]. A PCR test device typically consists of a thermoelectric cooler (TEC) and several reaction chambers [5]. In PCR device, a thermoelectric cooler maintains the temperature of the DNA tubes at some specific values (90°C, 55°C and 72°C) for a predetermined amount of time. Denaturation, renaturation and extension are three steps of a periodic cycle performed using PCR temperature control technology [6]. TEC is used to quickly perform these three-stage heating-cooling processes [7].

Robust and optimized controller design is essential to achieve a precise temperature control of the PCR device. Most studies in the literature have used PID or fuzzy logic based PID controllers for temperature control in PCR device [8]-[13] and their temperature control system models have been developed [8]-[11]. Ai-Xian et al. provided the fuzzy auto-adjust PID control method and the hardware and software design of the PCR temperature control system in comparison to the highlighted system characteristics [12]. Singh et al used Ziegler-Nichols tuning methods to find the PID controller's settings of the temperature control system [13]. Li et al. developed a fuzzy PID controller and compared it with a lead correction controller in order to optimize the thermal cycler performances of the microfluidic PCR system [14]. Dinca et al. presented the development of a PID controller that was used to swiftly and precisely manage the temperature of a PCR micro reactor in lab-on-a-chip research [15]. After determining the design objectives and considering the hardware constraints, the controller was developed using the root locus method to create a two-

This work is licensed under a Creative Commons Attribution 4.0 License. For more information, see https://creativecommons.org/licenses/by/4.0/

This article has been accepted for publication in IEEE Access. This is the author's version which has not been fully edited and
content may change prior to final publication. Citation information: DOI 10.1109/ACCESS.2024.3392734

degree-of-freedom continuous time controller and place the dominant pole pair [15]. Kim et al. created a continuous flow polydimethylsiloxane based microfluidic PCR using two heat block zones and a PID temperature control system as a universal platform for gene amplification [16]. It was obtained better results using a PID controller than using a manual method. [16]. Katja et al. developed the planning, development, and testing of a real-time, affordable, portable PCR device that may be used in resource-constrained and emergency medical settings [17]. Khnouf et al. designed and optimized the Rayleigh Bénard convection-based PCR microchip. In order to perform PCR effectively, the heater was managed using a PID controller [18]. Liu et al. published an adaptive PCR temperature management algorithm based on hybrid fuzzy PID controller, which parameter values were determined by the relay self-tuning algorithm [19]. Jun et al. proposed a smith fuzzy PID controller by fusing the Smith predictor with a fuzzy PID controller in order to combat models with big inertia and large hysteresis with the application of the heat transfer theory [20].

In the literature, apart from classical PID and fuzzy logic based PID control strategies, other methods have been proposed for temperature control of various PCR devices. For example, a nucleic acid amplification system was developed based on PCR [21]. For the control of this system, the authors suggested the integral separation PID algorithm, and a support vector regression (SVR) based intelligent temperature control technique [21]. Nasser et al. proposed the adaptive fuzzy logic controller and bang-bang as a hybrid controller, the temperature control system in PCR is managed to give good precision at the fastest rate of change of temperature possible [22]. Shan et al. constructed a small thermoelectric cooler-based continuous temperature control system, and this study has proposed a novel method for figuring out the system's transfer function since the system is a big time-delay control system [23]. Zhang et al. discussed fuzzy neural network controller in PCR reactor [24]. Jun et al. proposed an experimental control algorithm based on the predicative control techniques after examining the characteristics of a PCR temperature control system [25]. In addition, various optimization techniques are widely used for controller designs of many systems in the literature. Ekinci et.al proposed the controller system Aquila optimizer via chaotic local search and modified opposition-based learning strategies for vehicle cruise control system [26]. On the other hand, a new goal function and modified Aquila optimizer algorithm were developed to construct a PIDD^2 controlled automatic voltage regulator system effectively [27]. Tabakh and Tiryaki proposed an artificial intelligence method for predicting the optimum parameters of proportional-integral-derivative controller in an automatic voltage regulator system [28]. Snásel et al. proposed an integrated optimization technique for power system stabilization that combines the weighted mean of vectors optimizer with chaotic-orthogonal-based learning and basic Gaussian strategies for a single-machine infinite-bus system in the power system stabilizer model [29].

PCR temperature control systems (TEC) are usually mathematically modeled in the form of a transfer function, including the temperature delay of the system due to heat transfer [8]-[12]. The Pade approximation allows a rational transfer function to modify a pure time delay. However, obtaining a set of PID controller parameter values when employing low-order Pade approaches for the time delay can result in unstable behavior of the closed-loop system. [30], [31]. A PID controller parameter set that is roughly near to the real set can be achieved by raising the order of the Pade technique, but this comes with a higher algebraic complexity that must be overcome [31]. To overcome these problems and find a complete set of PID controller parameters, a generalization of the Hermite-Biehler theorem is used in this study. The characteristic polynomials of the time-delay systems are known as quasi-polynomials. This is because quasi-polynomials have non-finite numbers of roots, stability analysis is quite challenging. Hermite-Biehler theorem for time-delay systems cannot be applied directly, but stability analysis can make use of a generalization of the theorem based on certain fundamental Pontryagin ideas for quasi-polynomials [31]-[34]. Furthermore, advanced control methods are used for stability analysis and applied to the real system [35]-[36].

The contributions of this study are summarized as follows:

Firstly, the mathematical model of the temperature management system of polymerase chain reaction (PCR) device using semiconductor cooler was obtained as a time-delayed transfer function using heat conduction theory to develop the dynamic differential equation of heat conduction. Subsequently, using the MATLAB system identification Toolbox, the parameter values of the transfer function with real-time measurements of the micro-TEC structure developed in our previous article [37] was obtained. In PCR device, extreme temperature changes can lengthen both the overshoot and the time it takes the TEC system to stabilize, making stability control extremely difficult. This paper combines stability and optimization in order to provide a PID control plan with the qualities of rapid temperature increase and fall, minimal overshoot, high precision, and high robustness. For this purpose, PID control of a thermoelectric cooler in the PCR device is proposed using a method combining stability and machine learning algorithm. A generalization of the Hermite-Biehler theorem is used to identify the regions of the PID controller that make the system robustly stable in closed-loop. In this article, a generalized Hermite-Biehler theorem is used to restrict the search space to a stable region, while machine learning is used to determine the optimal parameters of the PID controller, which makes the TEC system robustly stable. Therefore, a new dataset is obtained to compute the best value of the PID controller parameter that stabilizes the

This work is licensed under a Creative Commons Attribution 4.0 License. For more information, see https://creativecommons.org/licenses/by/4.0/

This article has been accepted for publication in IEEE Access. This is the author's version which has not been fully edited and content may change prior to final publication. Citation information: DOI 10.1109/ACCESS.2024.3392734

system. This dataset is constructed from the values at the stability region determined by the generalized Hermite-Biehler theorem. Then, the XGBoost algorithm [38] from the machine learning (ML) method is used to determine the best parameter values of the PID controller in this study. GridSearchCv in the scikit-learn library was used to perform the hyperparameter optimization of the XGBoost algorithm used in this study. GridsearchCV measured the model performance separately for each possible value of the predetermined parameter values and for each possible value of these parameters and identified the hyperparameters with the highest values. Using the determined hyperparameters, the model successfully accomplished the task of estimating the parameters of the PID controller. XGBoost Hyperparameters with GridSearchCV were used for the first time to predict PID controller parameters. To accomplish speedy analysis, the PCR procedure should be completed as quickly as possible. The fact that the RMSE, MSE and R^2 values representing the performance criterion values are 0.0685, 0.004 and 0.91, respectively, shows that our proposed method makes an accurate prediction. Moreover, the estimation time of the parameters of the PID controller took 3 seconds. Thus, it is observed that the XGBoost algorithm predicts quickly and accurately.

In this paper, a machine learning method based PID (ML-PID), several metaheuristic optimization algorithms known as the equilibrium optimization based PID (EO-PID) [39], the particle swarm based PID (PSO-PID) [40], the artificial bee colony based PID (ABC-PID) [41] are all utilized to obtain the controller settings. By applying optimal PID controller parameters to the system, the transient response performances of the output signals are compared. One of the reasons behind the use of various controller techniques is to determine the most effective method for system control. These processes help save time and reduce production costs. From the simulation results, it has been shown that the ML-PID controllers applied in the TEC system are compatible with the changing system conditions. Thus, the TEC system's performance can be observed and improvement, while errors can be minimized through optimization before production.

This paper is structured as follows: The mathematical model of the PCR device's temperature management system is described in Section 2. In Section 3, a generalization of the Hermite-Biehler theorem for the TEC in the PCR device is used to determine the region of stabilizing PID parameters. Determining the best ML-PID controller parameter from the data collection system in the Python environment is explained in Section 4. In Section 5, the fundamental phases of the XGboost algorithm are described in depth. The simulation results for the TEC system with PID controllers, which are optimized with the machine learning (ML), EO, PSO, ABC and ZN algorithms are compared in Section 6. Some concluding remarks are included in Section 7.

II. MODEL of TEMPERATURE CONTROL SYSTEM on PCR

The thermoelectric coolers (TEC) are the basic elements for temperature control of PCR. A TEC unicouple is basically formed from n- and p-types TE materials connected via an electrode, and a ceramic is placed on top, and bottom of the electrode as shown in Figure 1 [37]. The heating and cooling capabilities are mainly regulated by the current circulating through its circuit. Additionally, altering the direction of the loop current inverts its cold and hot terminals, facilitating swift heating and cooling of the blocks within the PCR device.

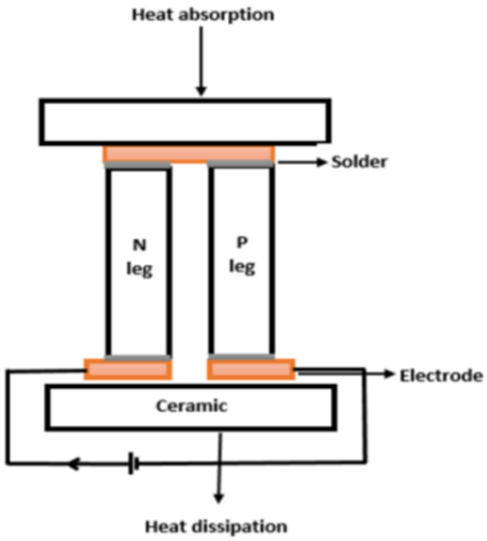


FIGURE 1. The temperature control system of PCR.

The Seebeck, Thomson, and Fourier effects have relatively little influence on the entire system, hence only the Peltier and Joule effects are considered in the analysis of the temperature control module [9]. The Peltier cooling is given as:

$$Q_p = \Pi_{pn} I \tag{1}$$

where Π_{pn} is Peltier coefficient and I is current. When an electric current flows through a conductor, the conductor's resistance obstructs the current flow and raises the conductor's temperature. The heat produced by the Joule effect is given as follows.

$$J_h = \frac{1}{2} I^2 R_i \tag{2}$$

R_i is the resistance. The Joule effect strongly depends on the electric current and internal resistance. The heat transfer by conduction loss is given as:

$$Q_l = K\,(T_1 - T_2) \tag{3}$$

where T_1 denotes the temperature at the semiconductor cooler's hot end and T_2 denotes the temperature at the cooler's cold end, K denotes the cooler's thermal conductance. Equation (4) provides the heat release by the TEC.

This work is licensed under a Creative Commons Attribution 4.0 License. For more information, see https://creativecommons.org/licenses/by/4.0/

This article has been accepted for publication in IEEE Access. This is the author's version which has not been fully edited and content may change prior to final publication. Citation information: DOI 10.1109/ACCESS.2024.3392734

$$Q = \Pi_{pn}\ I + \frac{1}{2}I^2R_i - K\ (T_1 - T_2) \tag{4}$$

Equation (4) can be expanded using Taylor series:

$$\Delta Q = f'(I)\Delta I + \frac{f''(I)\Delta I^2}{2!} + \cdots \tag{5}$$

$$\Delta I = I_2 - I_1 \tag{6}$$

where the function f is a function of the connection that relates Q and I. The current I is constant, hence ΔI is minimal. When the higher order term is neglected, equation (5) can be simplified as follows:

$$\Delta Q = f'(I)\Delta I = k_0\,\Delta I \tag{7}$$

where k_0 is the coefficient of heat exchange. Equation (3) can be represented as

$$Q_l = \frac{\Delta T}{\theta} \tag{8}$$

using the heat transfer concept. While ΔT is the temperature change, θ is the thermal resistance of the thermoelectric module. If equation (4) is rearranged, equation (9) is given as:

$$Q = C\frac{dT}{dt} + Q_l \tag{9}$$

where C is the heat capacity. If equations (5), (6), (7) and (8) are substituted in equation (9), we have

$$C\frac{d\Delta T}{dt} + \frac{\Delta T}{\theta} = k_0\,\Delta I \tag{10}$$

The Laplace transform of the last equation gives the following transfer function of the system [8].

$$G_0(s) = \frac{\Delta T}{\Delta I} = \frac{k_0}{Cs + \frac{1}{\theta}} = \frac{k}{Ts + 1} \tag{11}$$

The ultimate transfer function is given by equation (12) when the temperature lag of the system brought on by heat transfer is taken into account, adding the delay time L in the above formula.

$$G_0(s) = \frac{k}{Ts + 1}e^{-Ls} \tag{12}$$

In this study, the mathematical model of the micro-TEC, which we developed in [37], is obtained as a time-delayed transfer function by analyzing the heat conduction theory and establishing the dynamic differential equation of heat conduction and is given in equation (12). To find the parameter values of equation (12), data were first taken from the experimental setup shown in Figure 2. Figure 2 consists of power supply, relay, micro-TEC, temperature sensor, current sensor and microcontroller. Temperature values in the TEC system at different voltage values were recorded with the microcontroller.

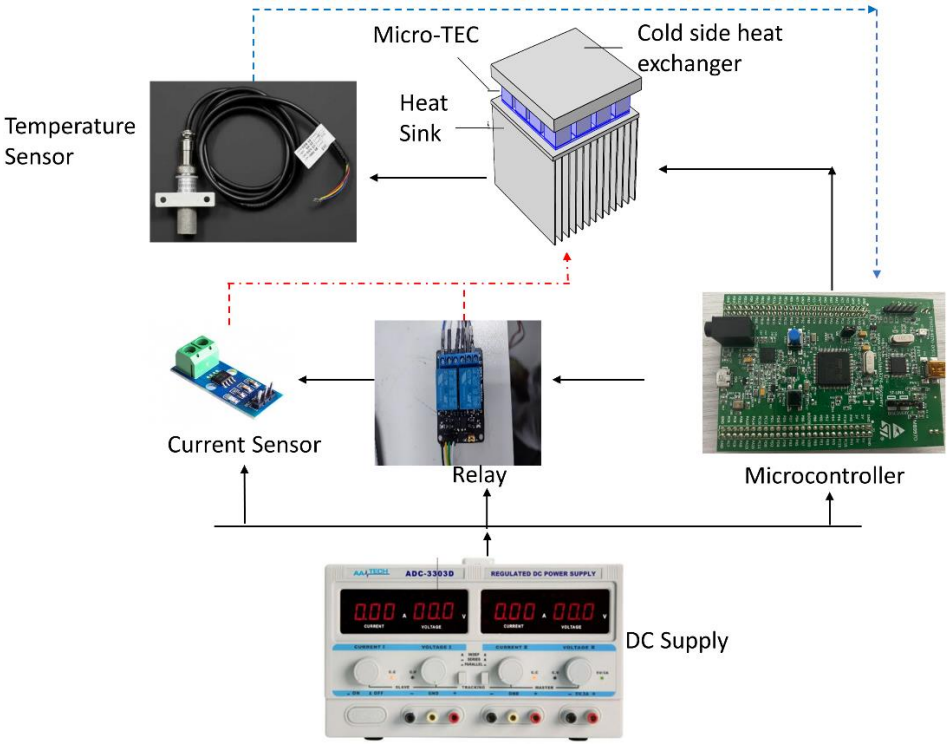


FIGURE 2. Experimental setup.

This work is licensed under a Creative Commons Attribution 4.0 License. For more information, see https://creativecommons.org/licenses/by/4.0/

This article has been accepted for publication in IEEE Access. This is the author's version which has not been fully edited and content may change prior to final publication. Citation information: DOI 10.1109/ACCESS.2024.3392734

Relays were used to change the polarity of the data coming to the heating-cooling elements and a switch was used to control the application time of the current coming from the source. Then, MATLAB system identification (SI) toolbox [42]-[43] was used to determine the parameters of the data obtained from the experiment. Using the experimental data, the mathematical model was created for this study with the help of MATLAB system identification toolbox. The transfer function of the control system of the thermoelectric model used in the PCR device is given as follows:

$$G_0(s) = \frac{60}{20.25s + 1} e^{-1.5s} \tag{13}$$

By using the MATLAB system definition toolbox, the transfer function with a validation percentage of 99.7% given in equation (13) was obtained.

III. STABILITY REGION CALCULATION BASED on HERMITE-BIEHLER THEOREM

In this section, the time-delayed mathematical model of TEC given by equation (13) is used to derive the set of stabilizing PID parameters using a generalization of the Hermite-Biehler theorem. Without knowing a real polynomial's roots, the traditional Hermite-Biehler Theorem can be utilized to calculate its Hurwitz stability [31], [32]. The classical Hermite-Biehler Theorem states that the necessary and sufficient conditions for a given real polynomial to be Hurwitz stability are that a certain interlacing property is satisfied.

Theorem 3.1. (The Classical Hermite-Biehler Theorem) [31]: $\delta(s) = \delta_0 + \delta_1 s + \ldots + \delta_n s^n$ is an n-degree real polynomial. If we write the polynomial $\delta(s)$ as follows, $\delta_e(s^2)$ and $s\delta_o(s^2)$ are the components of δ(s) formed by the even and odd powers of s, respectively.

$$\delta(s) = \delta_e(s^2) + s\delta_o(s^2) \tag{14}$$

If $s = jw$ is substituted in equation (14), it becomes $\delta(jw) = p(w) + jq(w)$. Here, $p(w) = \delta_e(-w^2)$ and $q(w) = w\delta_o(-w^2)$. While $w_{e_1}, w_{e_2}, \ldots$ denote non-negative real zeros of $\delta_e(-w^2)$, $w_{o_1}, w_{o_2}, \ldots$ represents the non-negative real zeros of $\delta_o(-w^2)$. If the following necessary and sufficient conditions are satisfied, the δ(s) polynomial provides interlacing property and is Hurwitz stable.

i.) The coefficients of the highest order terms of $\delta_e(-w^2)$ and $\delta_o(-w^2)$ have the same sign.
ii.) All the zeros of $\delta_e(-w^2)$ and $\delta_o(-w^2)$ are real and distinct, and non-negative real zeros satisfy the interlacing property as $0 < w_{e_1} < w_{o_1} < w_{e_2} < w_{o_2} < \cdots$

A. DETERMINATION OF STABLE REGION FOR PID TYPE CONTROLLER USING A GENERALIZATION OF FOR QUASI POLYNOMIALSIALS

First, the Ziegler-Nichols step response approach is presented in this section for setting PID controller parameters in time delay systems. Then, a generalization of the Hermite-Biehler Theorem for quasi-polynomials is examined. Figure 3 depicts a single input-single output control system controlled by a PID controller.

In the PCR temperature control system, $G_0(s)$ expresses the mathematical model of equation (12), and $F(s)$ is the PID controller in Figure 3. The PID controller is given as follows:

$$F(s) = k_p + \frac{k_i}{s} + k_d s \tag{15}$$

where, k_P, k_i and k_d are the proportional, integral and derivative gain parameters of the controller, respectively. In the Ziegler-Nichols step response method, the controller parameters are determined according to the values obtained from the open loop step response of the system [44]. By using a and L parameters, derived from the plant's step response, this method first characterizes the plant [31], [44].

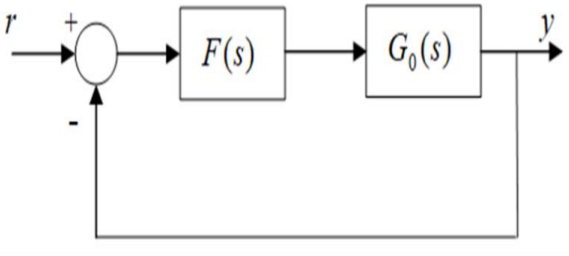


FIGURE 3. Closed-loop system with PID controller.

The parameter a is defined as follows.

$$a = k\frac{L}{T} \tag{16}$$

The PID controller parameters can be generated using the following formulas after determining a and L:

$$k_p = \frac{1.2}{a}, \qquad k_i = \frac{0.6}{aL}, \qquad k_d = \frac{0.6L}{a} \tag{17}$$

It is aimed to analytically determine the k_P, k_i and k_d PID controller parameters that stabilize the closed loop system in Figure 2. If the time delay L is equal to zero, the closed-loop characteristic equation $\delta(s)$ is given as follows.

$$\delta(s) = (T + kk_d)s^2 + (kk_p + 1) + kk_i \tag{18}$$

To ensure that the plant is stable in an open-loop, let us suppose that k and T are positive. Then, the following conditions can be written for the PID controller parameters

$$k_i > 0, \quad k_p > -1/k, \quad k_d - T/k \tag{19}$$

When the time-delay is different from zero, i.e., $L \neq 0$, the closed-loop characteristic equation of the time-delay system is as follows:

$$\delta(s) = (kk_i + kk_p s + kk_d s^2)e^{-Ls} + (1 + Ts)s \tag{20}$$

This work is licensed under a Creative Commons Attribution 4.0 License. For more information, see https://creativecommons.org/licenses/by/4.0/

This article has been accepted for publication in IEEE Access. This is the author's version which has not been fully edited and content may change prior to final publication. Citation information: DOI 10.1109/ACCESS.2024.3392734

Equation (20) is a quasi-polynomial and its number of roots is infinite. To find the stabilized PID controllers, we rewrite equation (20) in the following form as

$$\delta^*(s) = e^{Ls}\delta(s) = kk_i + kk_p s + kk_d s^2 + (1+Ts)se^{Ls} \tag{21}$$

Substituting $s = j\omega$ and $e^{jL\omega} = \cos(L\omega) + jsin(L\omega)$, we have

$$\delta^*(j\omega) = \delta_r(j\omega) + j\delta_i(j\omega) \tag{22}$$

where

$$\delta_r(\omega) = kk_i - kk_d\omega^2 - \omega\sin(L\omega) - T\omega^2\cos(L\omega) \tag{23}$$

$$\delta_i(\omega) = \omega\left[kk_p + \cos(L\omega) - T\omega\sin(L\omega)\right] \tag{24}$$

$T > 0$ for the system to be open loop stable. As seen from equation (23) and (24), while k_i ve k_d affect $\delta_r(\omega)$, k_p affects only $\delta_i(\omega)$. Substituting $\omega = \frac{z}{L}$ into (23) and (24), we have,

$$\delta_r(z) = kk_i - \frac{kk_d}{L^2}z^2 - \frac{1}{L}z\sin(z) - \frac{T}{L^2}z^2\cos(z) \tag{25}$$

$$\delta_i(z) = \frac{z}{L}\left[kk_p + \cos(z) - \frac{T}{L}z\sin(z)\right] \tag{26}$$

From $\delta_i(z) = 0$, the following two equations can be written for the roots of the imaginary part:

$$z = 0 \tag{27}$$

$$kk_p + \cos(z) - \frac{T}{L}z\sin(z) = 0 \tag{28}$$

We see that one of the roots of $\delta_i(z)$ is $z_0 = 0$. Other roots are difficult to find, because (28) needs to be solved analytically. In this case, we can plot (28) and examine the result graphically. The plot $kk_p + \cos(z)/\sin(z)$ is intersected by the $\frac{T}{L}z$ line. If the z values at these intersections are represented as α_i $(i = 1,2,\ldots.)$, we can write the following for the first $z = \alpha_1 \in (0,\pi)$ [31].

$$\frac{kk_p + \cos(\alpha_1)}{\sin(\alpha_1)} = \frac{T}{L}\alpha_1 \tag{29}$$

At $z = \alpha_1$, the $\frac{T}{L}z$ line is tangent to the plot of $\frac{kk_p+\cos(z)}{\sin(z)}$. Taking the first derivative of (29) with respect to $z = \alpha_1$, we calculate

$$1 + kk_p\cos(\alpha_1) = -\frac{T}{L}\sin^2(\alpha_1) \tag{30}$$

If we rewrite (29) for $z = \alpha_1 \in (0,\pi)$, we find

$$kk_p = \frac{T}{L}\alpha_1\sin(\alpha_1) - \cos(\alpha_1) \tag{31}$$

Substituting (31) in (29), this allows us to obtain the following equation.

$$\begin{aligned} 1 + \left[\frac{T}{L}\alpha_1\sin(\alpha_1) - \cos(\alpha_1)\right]\cos(\alpha_1) \\ = 1 - \underbrace{\cos^2(\alpha_1)}_{\sin^2(\alpha_1)} + \frac{T}{L}\alpha_1\sin(\alpha_1)\cos(\alpha_1) \\ = -\frac{T}{L}\sin^2(\alpha_1) \end{aligned} \tag{32}$$

When equation (32) is rearranged, we obtain

$$\frac{T}{L}\alpha_1\cos(\alpha_1) = \sin(\alpha_1)\left(-\frac{T}{L} - 1\right) \tag{33}$$

We obtain $\alpha_1 \in (0,\pi)$ as a solution of the subsequent equation from this last equation.

$$\tan(\alpha_1) = \frac{\sin(\alpha_1)}{\cos(\alpha_1)} = -\frac{T}{T+L}\alpha_1 \tag{34}$$

Thus, the stabilizing PID gain regions for first-order systems with time delays as in (12) can be found using the following theorem [31].

Theorem 3.2 [31]: To solve the PID stabilization problem of an open-loop stable time-delay system with transfer function $G_0(s)$ as in (12), with $T > 0$, $k > 0$ and $L > 0$, the set of k_p values is found with the following condition. $\delta_i(w)$ has only real roots if and only if

$$-\frac{1}{k} < k_p < \frac{1}{k}\left[\frac{T}{L}\alpha_1\sin(\alpha_1) - \cos\alpha_1\right] \tag{35}$$

where α_1 is the solution of the equation

$$\tan(\alpha) = -\frac{T}{T+L}\alpha \tag{36}$$

in the interval $(0,\pi)$.

♦

After calculating the $k_p$values from Theorem 3.2, to find the $k_i - k_d$ regions for z≠0, let us rewrite $\delta_r(z)$ as follows:

$$\delta_r(z) = \frac{k}{L^2}z^2\left[-k_d + \frac{L^2}{z^2}k_i - \frac{L}{kz}\left(\sin(z) + \frac{T}{L}z\cos(z)\right)\right] \tag{37}$$

From (37), for z≠0, the real part $\delta_r(z)$ can be rewritten as

$$\delta_r(z) = \frac{k}{L^2}z^2[-k_d + m(z)k_i + b(z)] \tag{38}$$

where

$$m(z) \triangleq \frac{L^2}{z^2}, \qquad b(z) \triangleq \frac{L}{kz}\left[\sin(z) + \frac{T}{L}z\cos(z)\right] \tag{39}$$

Thus, the following Lemma can be given to find the $k_i - k_d$ regions [31].

Lemma 3.1: The necessary and sufficient conditions on k_i and k_d for the roots of $\delta_r(z)$ and $\delta_i(z)$ to interlace for

This work is licensed under a Creative Commons Attribution 4.0 License. For more information, see https://creativecommons.org/licenses/by/4.0/

This article has been accepted for publication in IEEE Access. This is the author's version which has not been fully edited and content may change prior to final publication. Citation information: DOI 10.1109/ACCESS.2024.3392734

each value of k_p in the range indicated by (35) are the following infinite set of inequalities.

$$\left.\begin{array}{l} k_i > 0 \\ k_d > m_1 k_i + b_1 \\ k_d < m_2 k_i + b_2 \\ k_d > m_3 k_i + b_3 \\ \vdots \end{array}\right\} \quad (40)$$

where the parameters m_j and b_j *for* $j = 1,2,3,\ldots$ are given by

$$m_j \cong m(z_j) \quad (41)$$

$$b_j \cong b(z_j) \quad (42)$$

♦

In this article, a generalization of the Hermite-Biehler theorem is employed to compute the set of stabilizing PID parameters using the time-delayed mathematical model of micro-TEC provided by equation (13). The micro-TEC transfer function parameters are *k*=60, *T*=20.25 and *L*=1.5. We need to determine the answer to the $tan(\alpha) = -0.931034\alpha$ using equation (36) in Theorem 3.2. To create the graphs in Figure 4, we graph $tan(\alpha)$ and -0.931034α in this case. From Figure 4, we obtain $\alpha_1 = 2.05284$ by solving $tan(\alpha) = -0.931034$ in the interval $(0, \pi)$. From (35), the $\delta_i(w)$ has only real roots if and only if

$$-0.0167 < k_p < 0.416983 \quad (43)$$

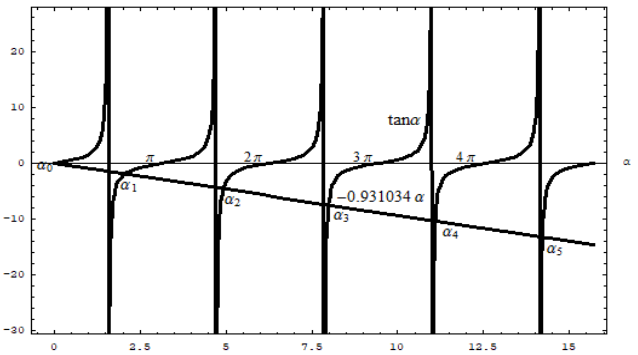


FIGURE 4. Plot of $tan(\alpha) = -0.931034\alpha$

Calculating the PID controller parameter k_p using equations (16) and (17), we have $k_p = 0.27$. Let's set the PID controller parameter k_p to value of 0.27, which is within the interval in equation (43). For $k_p = 0.27$, equation (28) takes the form

$$16.2 + \cos(z) - 13.5z \sin(z) = 0 \quad (44)$$

If we plot $16.2 + cos(z)$ and $13.5z\ sin(z)$ in the previous equation to find the positive real roots of (44), we get Figure 5. As seen in Figure 5, the $16.2 + Cos(z)$ and $13.5z\ sin(z)$ curves intersect. When we calculate a few of the positive real roots of equation (44) from Figure 5 and arrange them in ascending order of magnitude, we have

$$z_1 = 1.2764, z_2 = 2.7105, z_3 = 6.4808, z_4 = 9.3034 \quad (45)$$

Using (41), (42) and (45), we calculate the parameters m_j and b_j for $j = 1,2,3,4$:

$$\left.\begin{array}{ll} m_1 = 1.38103 & b_1 = -0.11667 \\ m_2 = 0.306264 & b_2 = 0.302762 \\ m_3 = 0.0535698 & b_3 = -0.331686 \\ m_4 = 0.0259956 & b_4 = 0.334692 \end{array}\right\} \quad (46)$$

when the following inequalities are satisfied, interlacing the roots of the real and imaginary parts of $\delta^*(jw)$ occurs for $k_p = 0.27$ according to Lemma 3.1:

$$\left.\begin{array}{l} k_i > 0 \\ k_d > 1.38103 k_i - 0.11667 \\ k_d < 0.306264 k_i + 0.302762 \\ k_d > 0.0535698 k_i - 0.331686 \\ k_d < 0.0259956 k_i + 0.334692 \\ \vdots \end{array}\right\} \quad (47)$$

Figure 6 depicts the borders of these regions in (47)

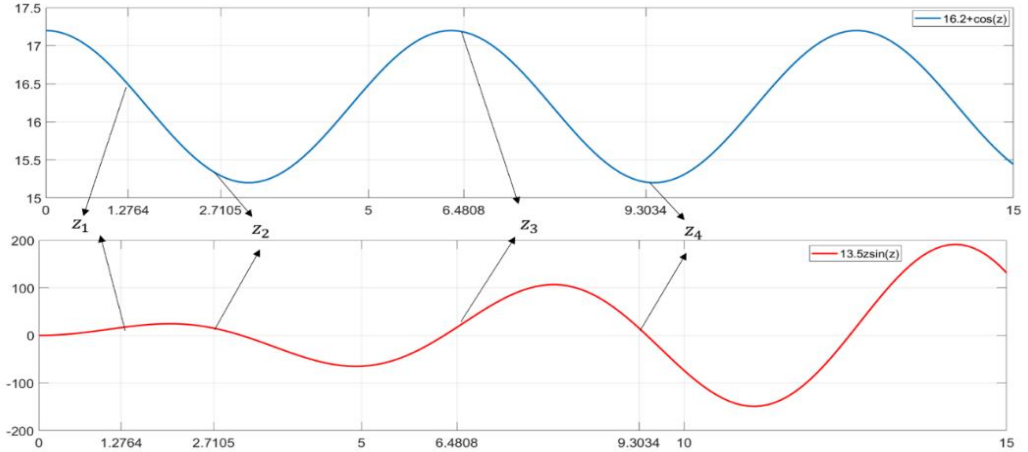


FIGURE 5. Plot of $16.2 + \mathbf{Cos(z)}$ and $\mathbf{13.5z\ sin(z)}$

This work is licensed under a Creative Commons Attribution 4.0 License. For more information, see https://creativecommons.org/licenses/by/4.0/

This article has been accepted for publication in IEEE Access. This is the author's version which has not been fully edited and
content may change prior to final publication. Citation information: DOI 10.1109/ACCESS.2024.3392734

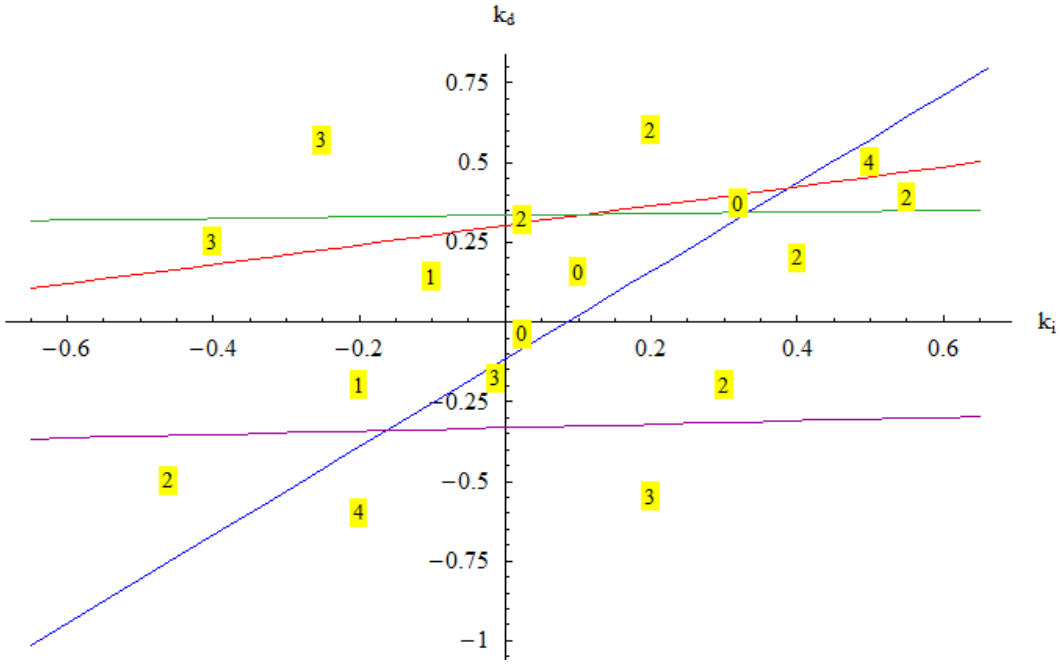


FIGURE 6. Stability Boundaries and Stability Region,

In Figure 6, $k_d = 1.38103k_i - 0.11667$, $k_d = 0.306264k_i + 0.302762$, $k_d = 0.0535698k_i - 0.331686$ and $k_d = 0.0259956k_i + 0.334692$ equations from (47) are shown in blue, red, purple and green colors, respectively. Unstable pole numbers for each region formed with the help of the inequalities in (47) in the k_i and k_d plane was written on them in Figure 6. The region where the number of unstable poles is zero gives all the k_i and k_d parameter values of the PID controller that will stabilize the TEC system.

IV. CONTROLLER IMPLEMENTATION

After obtaining the stability region of PID controllers by a generalization of the Hermite-Biehler theorem, a dataset is created to find the parameters of the best PID controller in the stability region. Then, the best PID controller parameters are obtained from the dataset with a machine learning method based PID (ML-PID) controller. In the proposed method, Figure 7 illustrates a data collection system. As depicted in Figure 7, it continuously records the set value for the TEC system to be controlled, along with error (*e*), the derivative of the error (*de*), *kp*, *ki*, *kd*, and output values. The value ranges for the controller parameters are determined using the generalized Hermite-Biehler theorem method, which is an important aspect of this study. Thanks to this approach, limit values for the controller parameters that stabilize the micro-TEC system have been determined. Once the stability region was determined, the TEC system operated within this region for a duration of 200 seconds with a sampling time of 0.1. The PID controller parameters were collected with kp fixed at 0.27 in MATLAB environment. As a result of the data collection simulation, 804 data were obtained within the stability region. The data set consists of *e*, *d*, *kp*, *ki*, *kd*, and output values. The best PID controller parameter was determined from the data set using machine learning algorithm in Python environment.

V. MATERIAL METHOD

Machine Learning works with numerical and categorical data and is divided into types according to whether the data it uses is labeled, unlabeled, or hybrid [45]. In this study, all values in the data set are labeled and numerical. Therefore, it has been taken to use a supervised learning method when selecting the model to be established and the XGBoost algorithm was used. The XGBoost algorithm is a method derived from the Gradient Boosting algorithm [46]. Basically, it works with decision tree logic like the Gradient Boosting algorithm, but it uses bagging and boosting methods. Both methods prevent overfitting and underfitting of the model and improve model performance [45]. The bagging expression extracts samples with k elements from the data set consisting of k data and introduces them to separate trees, thus creating a collective learning model. For the result, information is obtained from all tree structures. Boosting is basically the combination of weak models to form a strong model. Within the forest structure created by decision trees, each individual tree represents a distinct model. These trees learn from the errors of others and collectively make decisions, effectively engaging in an optimization process. For the final result, information is obtained from all tree structures. In the forest structure formed by decision trees, each tree has a different model.

This work is licensed under a Creative Commons Attribution 4.0 License. For more information, see https://creativecommons.org/licenses/by/4.0/

This article has been accepted for publication in IEEE Access. This is the author's version which has not been fully edited and content may change prior to final publication. Citation information: DOI 10.1109/ACCESS.2024.3392734

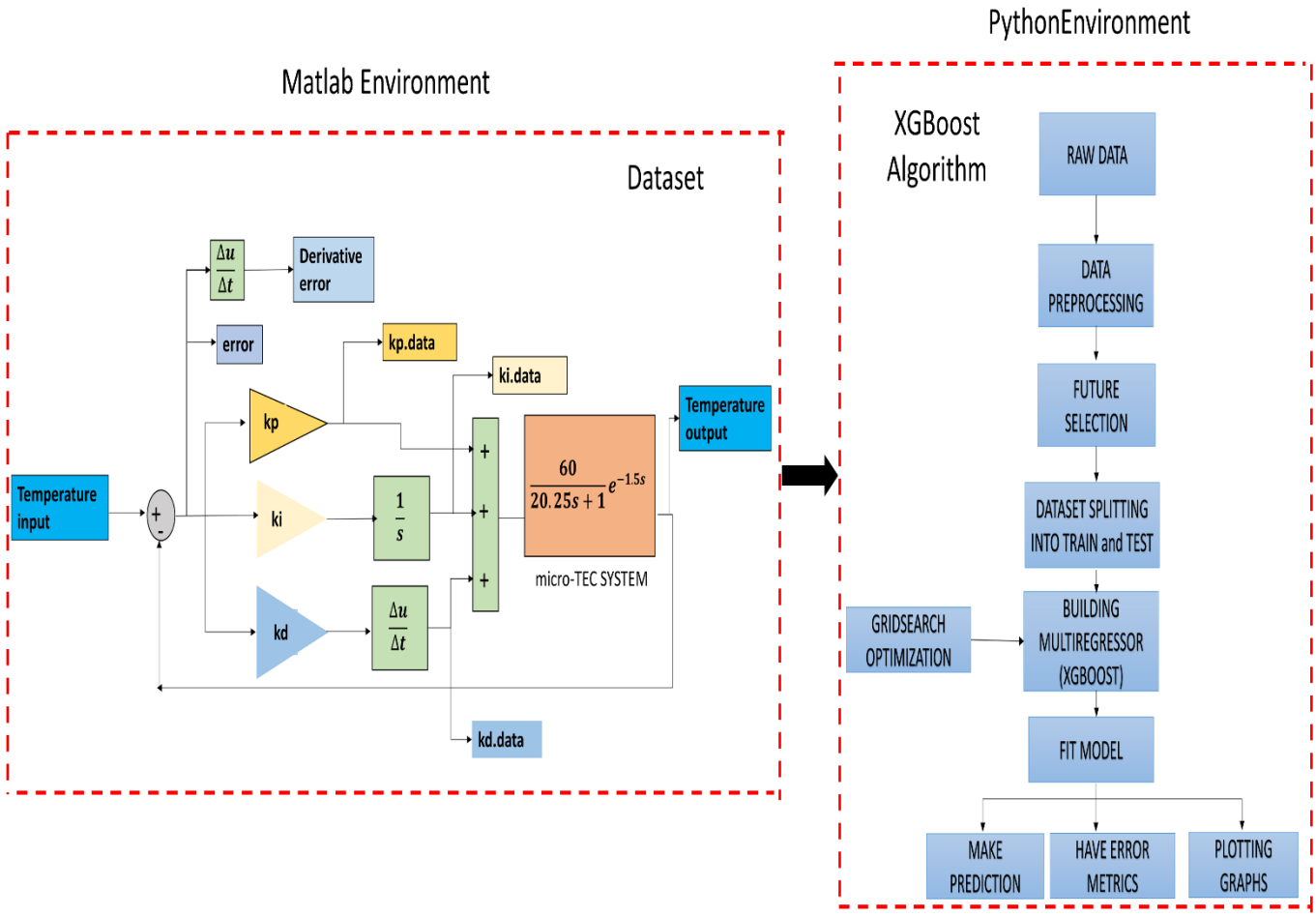


FIGURE 7. Data Collection System.

The aim of the XGBoost algorithm is to minimize the objective function at each iteration. Mathematical model of the XGBoost algorithm is given as

$$Obj\ Function = \sum_{i=1}^{n} l(y_i, \hat{y}_i) + \sum_{k=1}^{K} \Omega(f_k) \tag{48}$$

where, $\hat{y}$, y and $\Omega(f)$ are estimated value, real value and complexity structure of the decision tree, respectively. The first term of equation (48) is the training loss. The training loss determines how well the model adapts to the data during training. The second term given determines the regularization. The complexity and loss function of decision trees in XGBoost is as follows:

$$Loss\ Function = L(\theta) = \sum_i (\hat{y}_i - y_i)^2 \tag{49}$$

$$\begin{aligned} Complexity\ of\ Tree &= \Omega\big(f(t)\big) \\ &= \gamma T + \frac{1}{2}\lambda \sum_{j=1}^{T} w_j^2 \end{aligned} \tag{50}$$

where T: number of leaves, γ and λ are tree hyperparameters, w: Information weights on leaves.

The estimated value can be written as follows:

$$\hat{y}_i(t) = \sum_{k=1}^{t} f_k(x_i) = \hat{y}_i^{(t-1)} + f_t(x_i) \tag{51}$$

Substituting (51) in (48), we obtain

$$\begin{aligned} Obj\ Function^{(t)} = \sum_{i=1}^{n} \Big[& l\big(y_i, \hat{y}_i^{(t-1)}\big) + g_i f_t(x_i) \\ & + \frac{1}{2} h_i f_t^2(x_i) \Big] + \Omega(f_t) \end{aligned} \tag{52}$$

$$g_i = \partial_{\hat{y}^{(t-1)}} l(y_i, \hat{y}^{(t-1)}) \tag{53}$$

$$h_i = \partial^2_{\hat{y}^{(t-1)}} l(y_i, \hat{y}^{(t-1)}) \tag{54}$$

where g_i is first order derivative of the loss function and h_i is second order derivative of the loss function.

This work is licensed under a Creative Commons Attribution 4.0 License. For more information, see https://creativecommons.org/licenses/by/4.0/

This article has been accepted for publication in IEEE Access. This is the author's version which has not been fully edited and content may change prior to final publication. Citation information: DOI 10.1109/ACCESS.2024.3392734

(52) is rearranged, we have

$$Obj\ Function^{(t)} = \sum_{j=1}^{T}\left[G_j w_j + \frac{1}{2}(H_j + \lambda)w_j^2\right] + \gamma T \quad (55)$$

$$G_j = \sum_i g_i \quad , \quad H_j = \sum_i h_i \quad (56)$$

Equation (55) is the sum of quadratic functions from 1 to *T*. The value of each quadratic function and the value of the optimal weights are given as the following term

$$For\ each\ quadratic\ Function = G_j w_j + \frac{1}{2}(H_j + \lambda)w_j^2 \quad (57)$$

$$w_j^* = -\frac{G_J}{H_j + \lambda} \quad (58)$$

where w_j^* denotes the optimum weight value. Substituting (57) and (58) in (48), we obtain

$$\min Obj = -\frac{1}{2}\sum_{j=1}^{T}\frac{G_j^2}{H_j + \lambda} + \gamma T \quad (59)$$

Equation (59) is the minimum objective function. Equations (48) to (59) represent the mathematical model of the learning process of the XGboost algorithm. During training, the model is planned to estimate the controller parameters ki and kd according to the system output (*Y*), error (*e*), derivative of the error (*de*) and kp values, each of which are attributes. The flowchart of the learning phase of the XGBoost algorithm is illustrated in Figure 8. When Figure 8 is examined step by step, the main dataset, consisting of a total of 804 rows of data, was separated for training and testing by identifying labels. 70% of the total data was designated as training data and 30% as test data. The test and training data were determined randomly. While defining the XGBoost algorithm, which determines the originality of the study, the most appropriate parameter values were added to the model by making the necessary hyperparameter settings with GridSearchCV. These hyperparameters are 'learning_rate', 'max_depth', 'n_estimators' and 'base_score', respectively.

The learning_rate hyperparameter expresses the weights of the trees added during ensemble learning, in other words, the weights of the sub-algorithms. Small learning rates cause trees in the community to learn in more detail. It is used to prevent the model from overfitting.

The hyperparameter max_depth refers to the maximum depth of each tree. It determines the number of branches in the trees, in other words, the ability to learn the complexity of the model. Increasing this parameter too much will force the model to memorize rather than learn, causing it to overfit.

The n_estimators parameter determines the number of trees to be added to the model. More trees generally provides better performance, but increases computation time.

The base_score parameter determines the base estimate value. It is used in cases where the data set and the data are unevenly distributed and improves the performance of the model.

The GridSearchCV method used in this study tried all possible results for the hyperparameters given above one by one and obtained the most appropriate parameter values for the XGboost model. Thus, the model optimized itself by learning without memorizing. It is time for the model that obtains the best hyperparameter values to show performance. For the uniqueness of the research, the model was requested to learn two different correlation results simultaneously instead of learning a single correlation for the data during training. For this purpose, MultiOutputRegressor was defined in the base XGBoost model. The model trained itself with the data allocated for training and evaluated itself with test data that it had not seen before. In the last step of the algorithm, performance criteria are calculated on how well the machine learning models have learned and adapted to the data obtained.

Performance criteria are used to evaluate the efficiency of machine learning algorithm. In this study, correlation Coefficient (R^2), Root Mean Square Error (RMSE) and Mean Squared Error (MSE) values are used as performance criteria. All performance criteria are given as

$$RMSE = \sqrt{\frac{1}{n}\sum_{i=1}^{n}(y_i - \hat{y}_l)^2} \quad (60)$$

$$MSE = \frac{1}{n}\sum_{i=1}^{n}(y_i - \hat{y}_l) \quad (61)$$

$$R^2 = 1 - \frac{\sum_{l=1}^{n}(y_i - \hat{y}_l)^2}{\sum_{l=1}^{n}\left(y_i - \widehat{y_{avg}}\right)^2} \quad (62)$$

where, y_i, $\hat{y}_l$ and $(\widehat{y_{avg}})$ denote the desired output, the predicted output, and the average value, respectively. *n* represents the number of samples. The parameter estimation values of the PID controller are shown in Figure9(a) and Figure 9(b). In addition, the performance criteria values used in the XGBoost algorithm are given in Table 1. Table 1 shows that RMSE value is 0.0685 and MSE value is 0.004. The RMSE and MSE values are very close to zero, indicating that the model predicts well. In the regression task in machine learning models, the R^2 value used to understand the prediction performance of the model was found to be 91% which is an achievement. In addition, the error values of k_i and

This work is licensed under a Creative Commons Attribution 4.0 License. For more information, see https://creativecommons.org/licenses/by/4.0/

This article has been accepted for publication in IEEE Access. This is the author's version which has not been fully edited and content may change prior to final publication. Citation information: DOI 10.1109/ACCESS.2024.3392734

k_d are shown in Figure 10(a) and Figure 10(b), respectively. Each point represents a data sample. Error values are distributed between 0.1 and -0.2 in Figure 10(a) and Figure 10(b). Both Figure 10(a) and Figure 10(b) show that most values of errors are clustered on a line. Clustering on a line indicates that the predicted value is successful. Furthermore, Figure 11 displays the MSE curves and RMSE curves to illustrate the performance of the training and test datasets. Figure 11(a) shows the MSE curves of the training and test dataset. The MSE curves of the test and training datasets approach zero in Figure 11(a). Figure 11(b) illustrates the RMSE curves of the training and test dataset. Figure 11(b) shows that the RMSE values of the test and training datasets approach zero after each iteration.

TABLE 1. Model Performance Criteria.

Parameter	Values
R^2	% 91
RMSE	0.0685
MSE	0.004
Train accuracy	% 97

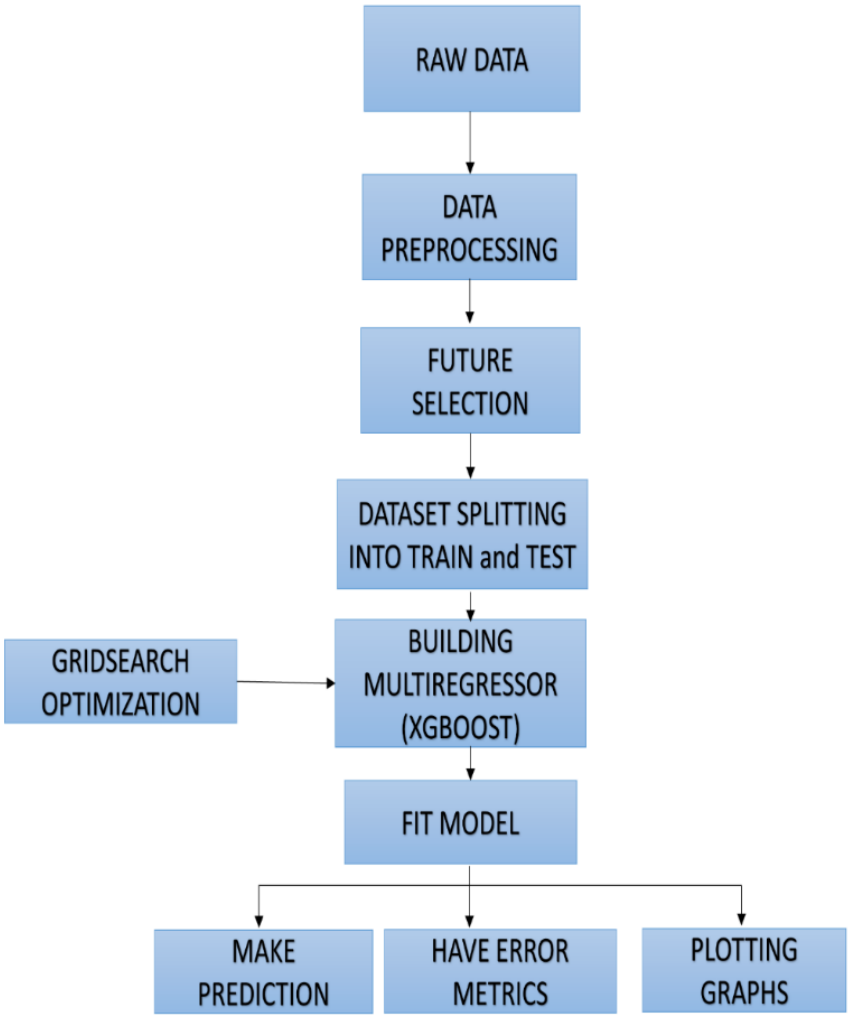


FIGURE 8. XGBOOST Flowchart

This work is licensed under a Creative Commons Attribution 4.0 License. For more information, see https://creativecommons.org/licenses/by/4.0/

This article has been accepted for publication in IEEE Access. This is the author's version which has not been fully edited and
content may change prior to final publication. Citation information: DOI 10.1109/ACCESS.2024.3392734

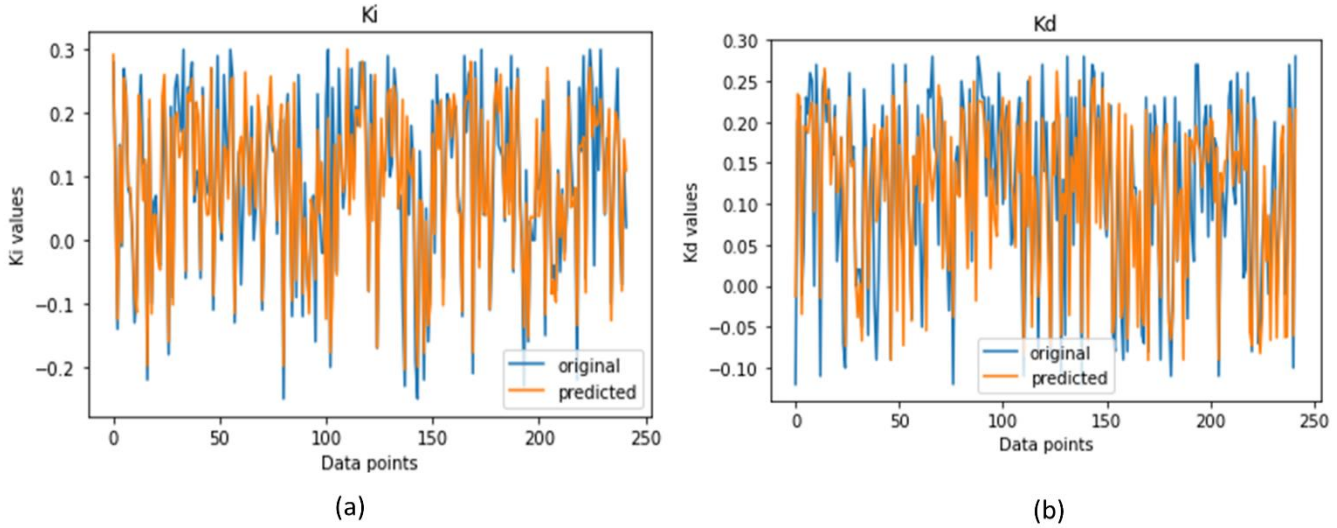


FIGURE 9. **(a) Estimation of k_i by XGBoost algorithm; (b) Estimation of k_d by XGBoost algorithm.**

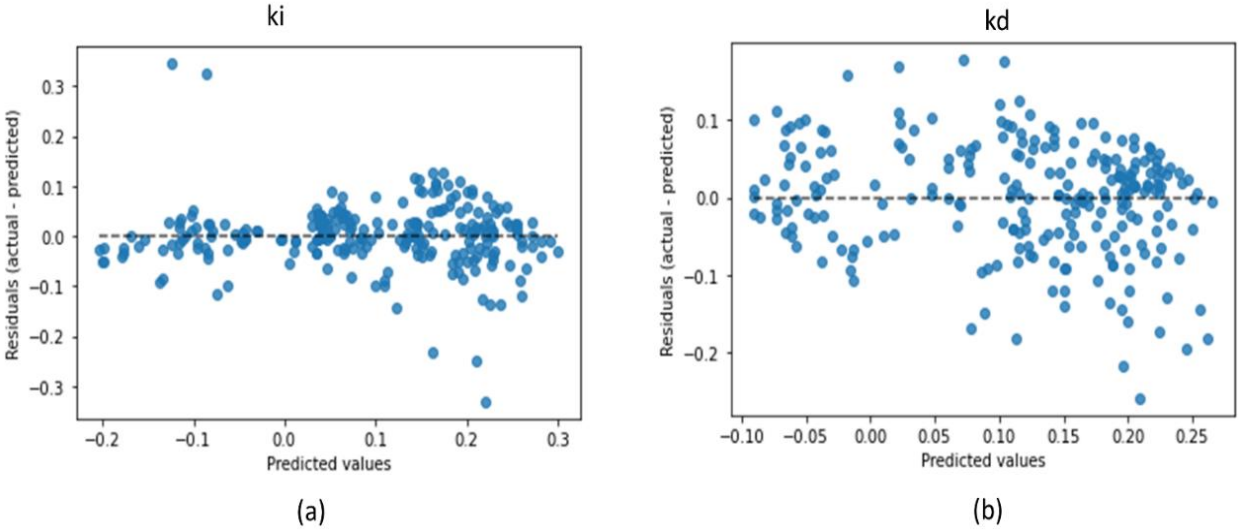


FIGURE 10. (a) Error values of k_i by XGBoost algorithm; (b) Error values of k_d by XGBoost algorithm.

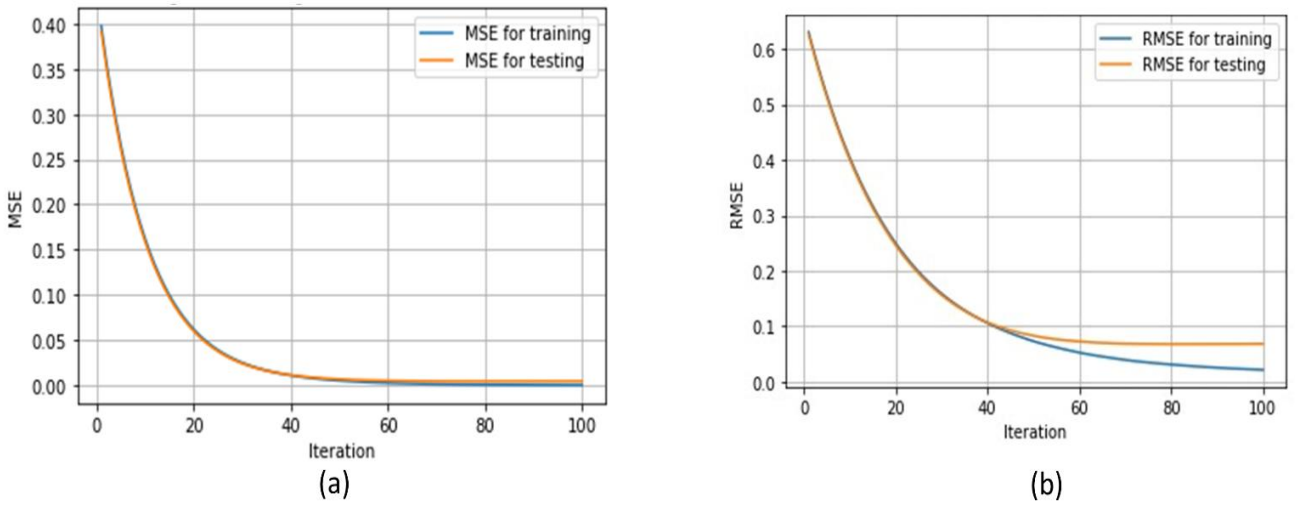


FIGURE 11. (a) MSE curve for training and test data; (b) RMSE curve for training and test data

This work is licensed under a Creative Commons Attribution 4.0 License. For more information, see https://creativecommons.org/licenses/by/4.0/

This article has been accepted for publication in IEEE Access. This is the author's version which has not been fully edited and content may change prior to final publication. Citation information: DOI 10.1109/ACCESS.2024.3392734

VI. SIMULATION RESULTS AND DISCUSSION

In this paper, the gain parameters of the PID controller in the micro-TEC system are obtained using both machine learning method and meta-heuristic optimization algorithms and the results are compared. Metaheuristic optimization algorithms search in regions where the TEC system is stable. These algorithms are Particle swarm optimization (PSO-PID), equilibrium optimization based PID (EO-PID), Artificial bee colony based PID (ABC-PID). All algorithms' calculations were performed on a single computer with a Windows 10 Intel® Core ™ I7-8565U 1.80 GHz CPU and 24 GB RAM. The results of the metaheuristic algorithms were obtained in MATLAB using the variable step ode15s. Integral time-weighted absolute error (ITAE) is the objective function used in this paper as follows:

$$ITAE = \int_0^\infty t|e|\,dt \tag{63}$$

where, t is time and e is error value. In a PCR device, as shown in Figure 12, the difference between the output value and the micro-TEC reference value constitutes the error value. The reason for using the ITAE objective function in the TEC system is to keep the error signal at a minimum level by approximating it closer to zero and to ensure that the settling time of the output signal is small with the controller effect. In this study, to reduce the objective function's value to its minimum, the metaheuristic optimization algorithms are used. When the value of the ITAE objective function is the smallest, the PID controller's optimal parameter values are found.

The parameter values of EO, PSO and ABC metaheuristic optimization algorithms are shown in Table 2.

TABLE 2. Parameter values of, EO, PSO and ABC optimization algorithms.

Parameter	Values
Population size	30
Iteration Number	30
Independent run number	30
Dimension	3
Lower bound	[0.1 0 -0.1]
Upper bound	[5 0.3 0.3]

The transient regimes of the output signals for different temperature inputs of the micro-TEC system, where optimized PID controllers are applied with these algorithms, were compared. The lower and upper boundary values of the PID controller parameters were obtained by a generalization of the Hermite-Biehler theorem. When machine learning method and metaheuristic methods are applied to PID controller at these range values, the best values of the PID controller are computed. Moreover, metaheuristic control strategies are used to the objective function to reach a minimum value. When the objective function has the smallest value, the parameter values of the PID controller are determined. The PID controller parameters obtained by both metaheuristic optimization algorithms and machine learning method are shown in Table 3. In addition, the convergence curves of the EO, PSO and ABC metaheuristic optimization algorithms for 30 iterations are shown in Figure 13.

TABLE 3. PID controller parameters found by metaheuristic algorithms.

Controller	k_p	k_i	k_d
PSO-PID	0.1677	0.0192	0.1620
ABC-PID	0.193	0.0045	0.1598
EO-PID	0.1120	0.013	0.11
ZN-PID	0.1951	0.0283	0.1015
ML-PID	0.27	0.03785529	0.00308238

The statistical performance measurements of these metaheuristic optimization algorithms are also given in Table 4. When these algorithms are compared in terms of standard deviations, mean values, and worst values, all algorithms have large values.

TABLE 4. Statistical performance measurements of EO, PSO and ABC optimization algorithms.

Measures	EO	PSO	ABC
Mean	8.027E+127	7.2E+127	2.2E+113
Standard deviation	1.740	7.2E+65	1.1E+112
Best value	0.011	0.037	0.111
Worst value	2.42E+129	4E+66	6.78E+114

The computation times of these metaheuristic optimization algorithms and machine learning method (ML) are given in Table 5. It can be seen from Table 5 that the machine learning method (ML) is faster than other algorithms.

TABLE 5. Computation times of Metaheuristic algorithms.

Measures	ML	EO	PSO	ABC
Computation Time (sec)	3	7440	480	7860

This work is licensed under a Creative Commons Attribution 4.0 License. For more information, see https://creativecommons.org/licenses/by/4.0/

This article has been accepted for publication in IEEE Access. This is the author's version which has not been fully edited and
content may change prior to final publication. Citation information: DOI 10.1109/ACCESS.2024.3392734

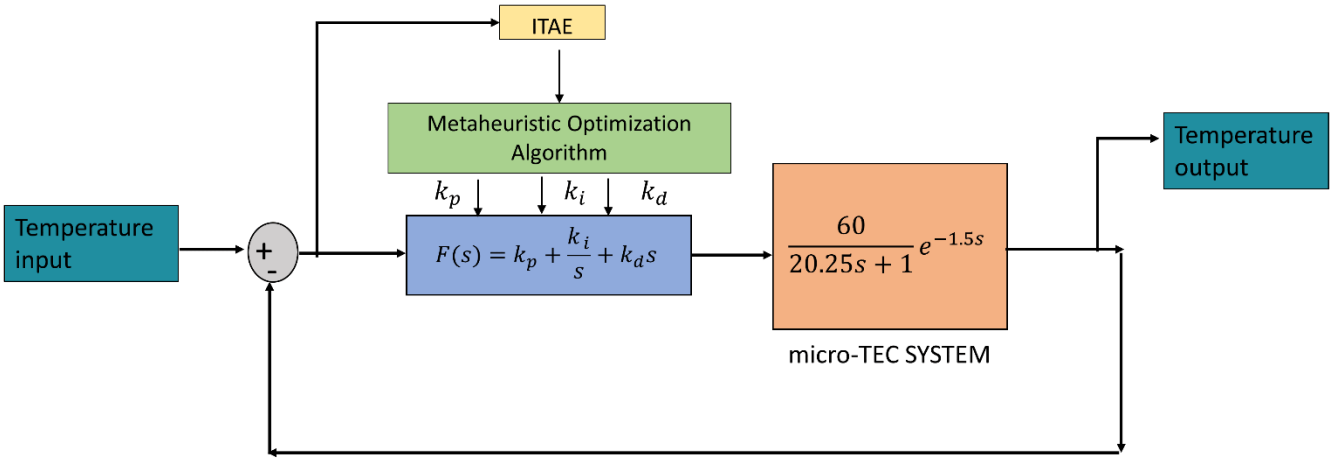


FIGURE 12. **Structure diagram of TEC model controlled by Metaheuristic Optimization Algorithms**

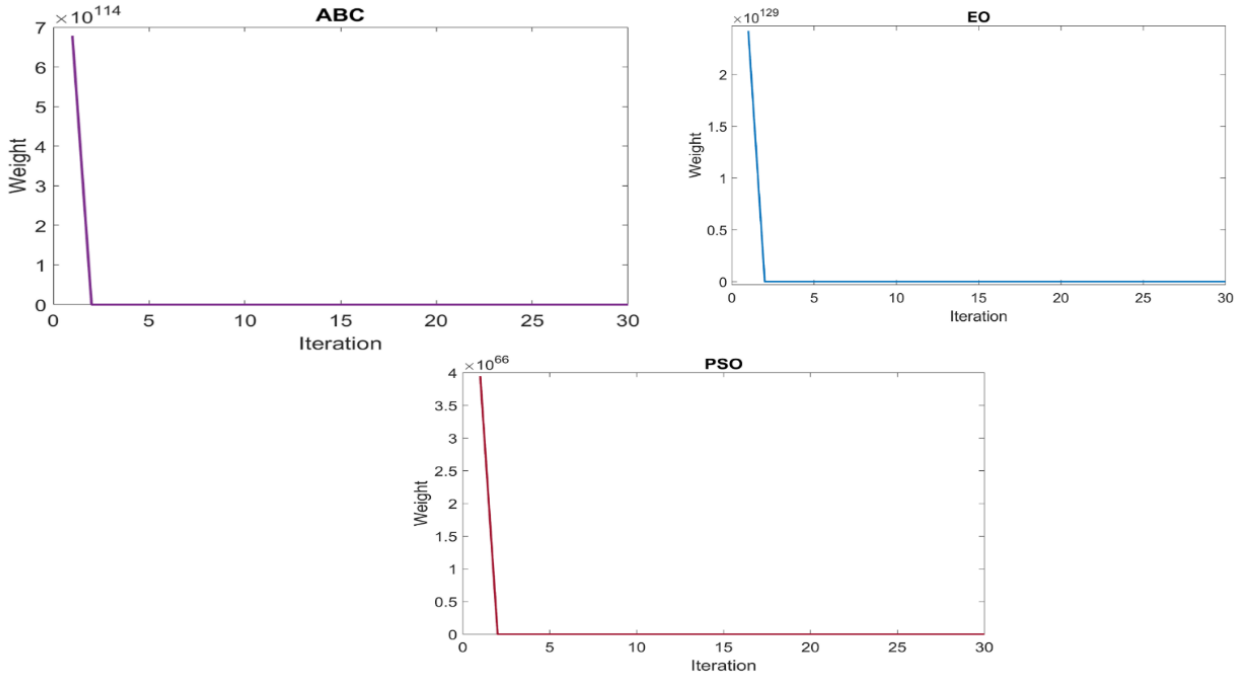


FIGURE 13. **Convergence curves of the metaheuristic algorithms**.

The output signals of the micro-TEC system with ML-PID, PSO-PID, ABC-PID, ZN-PID and EO-PID controllers applied in Table 6 are shown in Figure 14. In Figure 14, the reference, ML-PID, ZN-PID, PSO-PID, EO-PID, and ABC-PID are shown in green, yellow, blue, turquoise, and purple, respectively.

The zoomed output signals of this TEC system controlled by ML-PID, ZN-PID, EO-PID, PSO-PID and ABC-PID are for 0-40 seconds in Figure 15, for 40-80 seconds in Figure 16, for 80-120 seconds in Figure 17, for 120-160 in Figure 18 and for 160-200 seconds in Figure 19. In all figures, arrows indicate the settling times of these signals. We utilize the settling time and maximum over-shoot criteria to compare the performance of the optimized controllers. These comparison results are given in Table 6. A 5% band is used to determine the settling time in the transient behavior of the system's response signal.

This work is licensed under a Creative Commons Attribution 4.0 License. For more information, see https://creativecommons.org/licenses/by/4.0/

This article has been accepted for publication in IEEE Access. This is the author's version which has not been fully edited and
content may change prior to final publication. Citation information: DOI 10.1109/ACCESS.2024.3392734

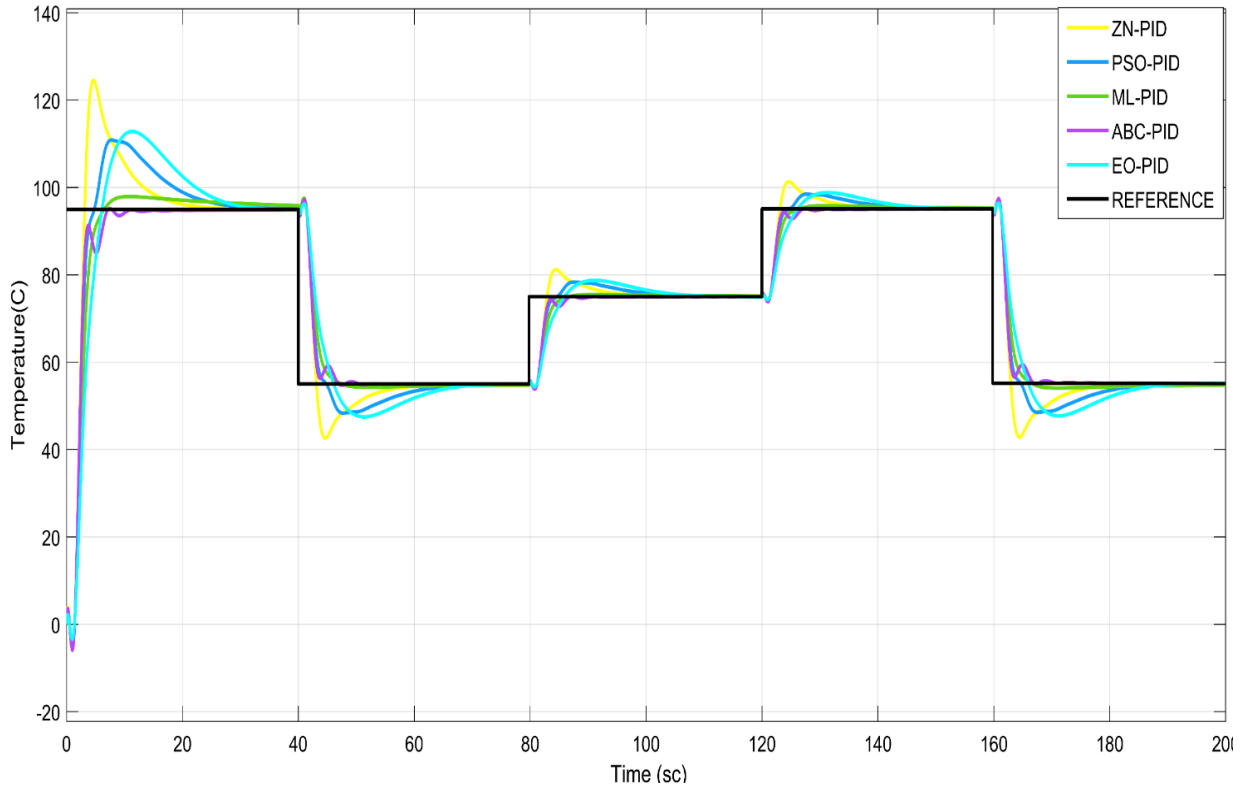


FIGURE 14. Output signals of micro-TEC system controlled by ML, ZN, EO, PSO and AB based PID controllers.

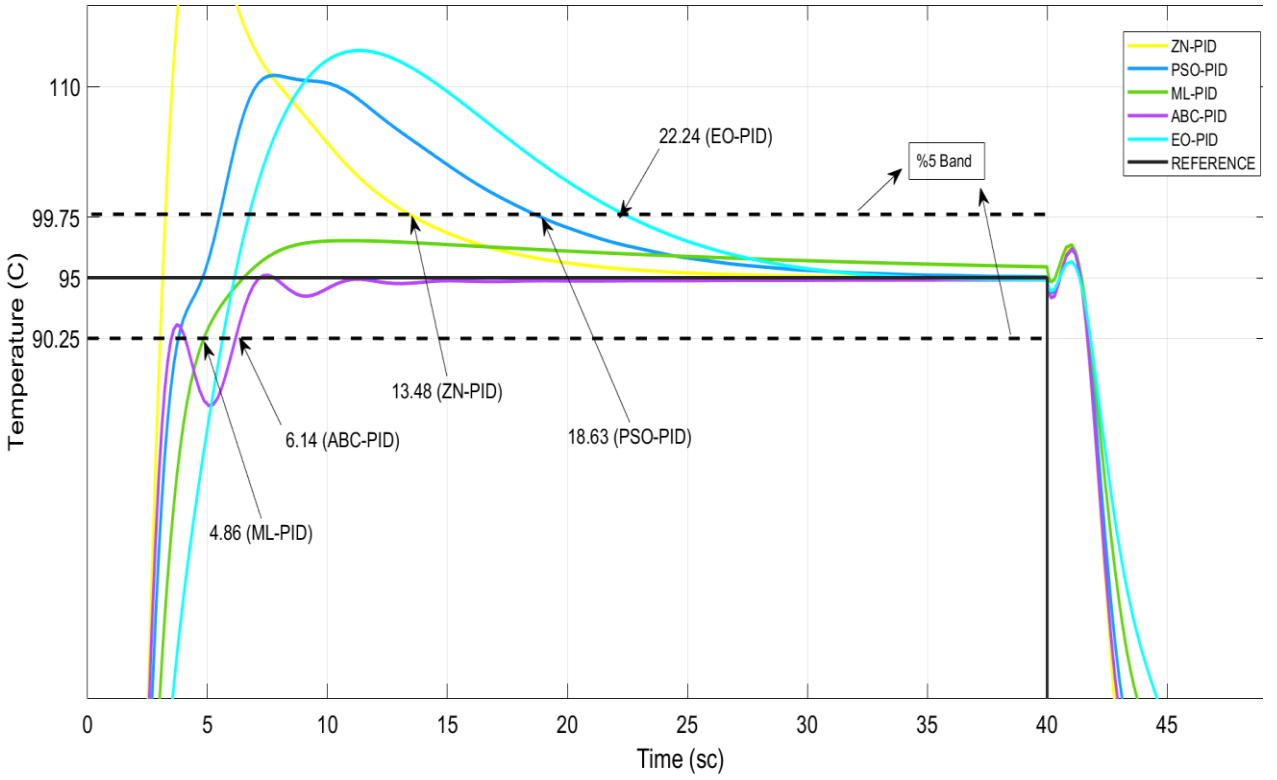


FIGURE 15. Output signals of the micro-TEC system between 0-40 seconds.

This work is licensed under a Creative Commons Attribution 4.0 License. For more information, see https://creativecommons.org/licenses/by/4.0/

This article has been accepted for publication in IEEE Access. This is the author's version which has not been fully edited and content may change prior to final publication. Citation information: DOI 10.1109/ACCESS.2024.3392734

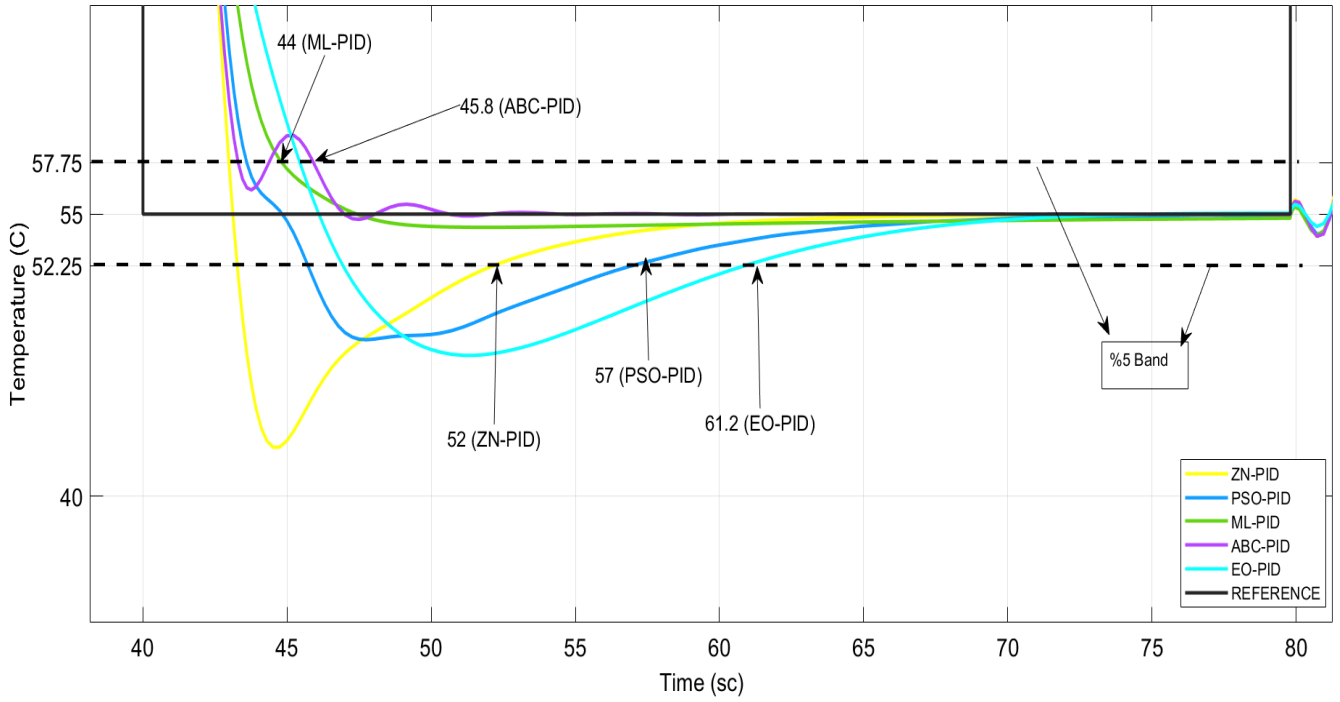


FIGURE 16. **Output signals of the micro-TEC system between 40-80 seconds.**

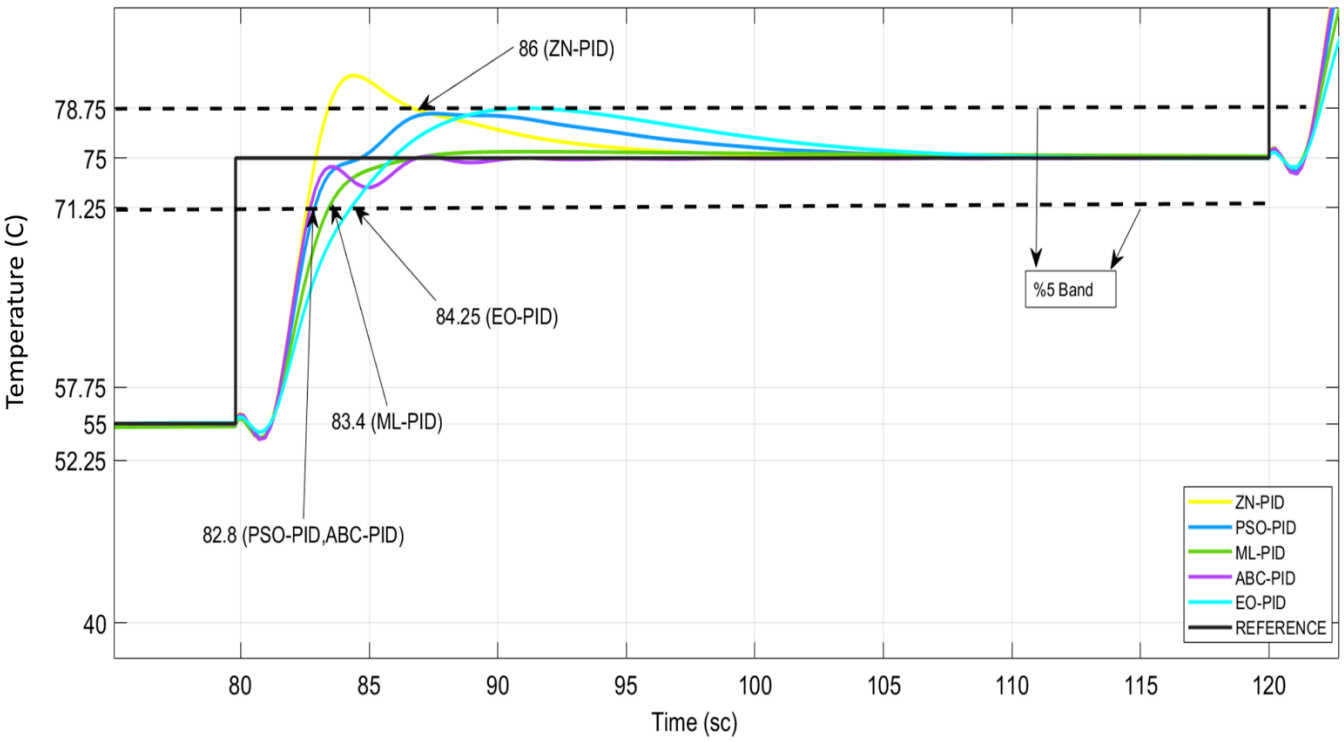


FIGURE 17. **Output signals of the micro-TEC system between 80-120seconds.**

This work is licensed under a Creative Commons Attribution 4.0 License. For more information, see https://creativecommons.org/licenses/by/4.0/

This article has been accepted for publication in IEEE Access. This is the author's version which has not been fully edited and content may change prior to final publication. Citation information: DOI 10.1109/ACCESS.2024.3392734

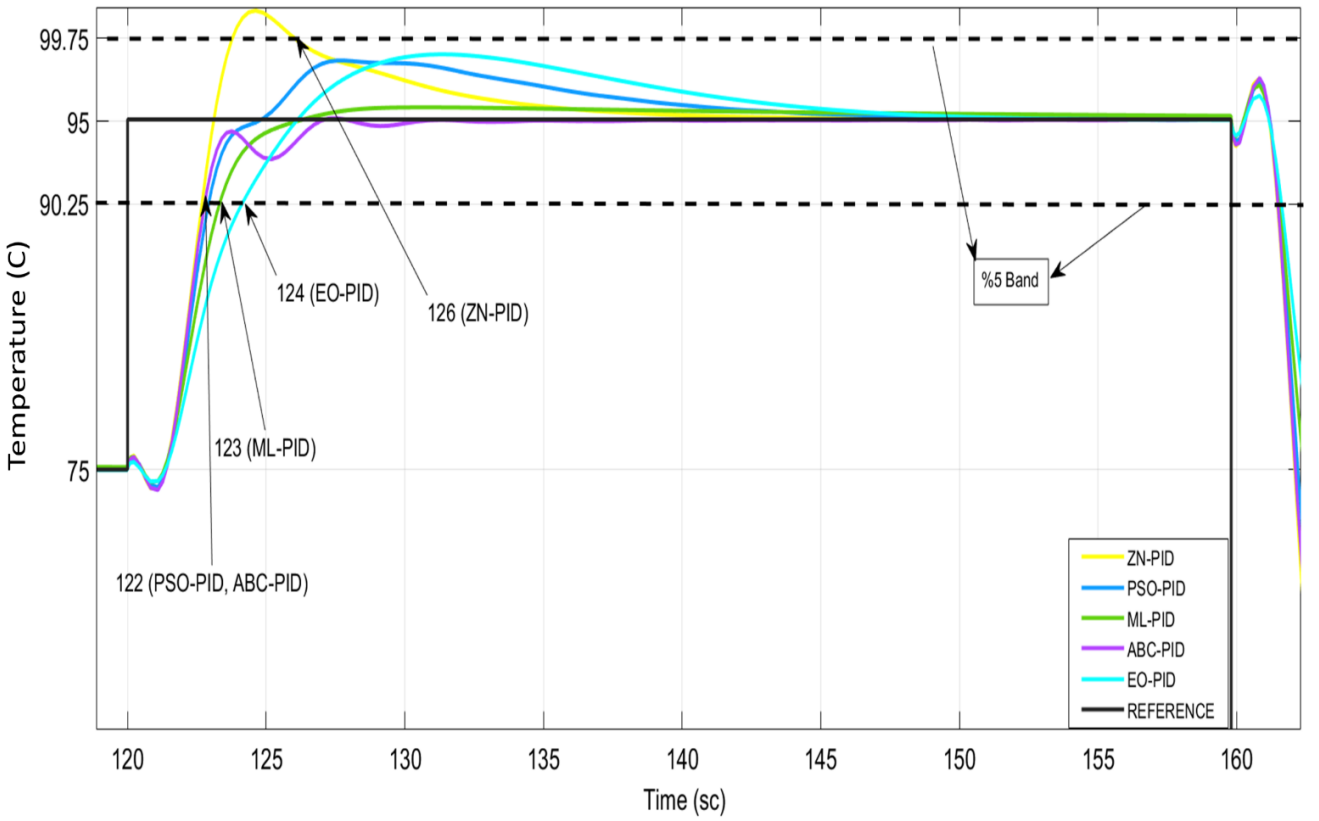


FIGURE 18. **Output signals of the micro-TEC system between 120-160 seconds.**

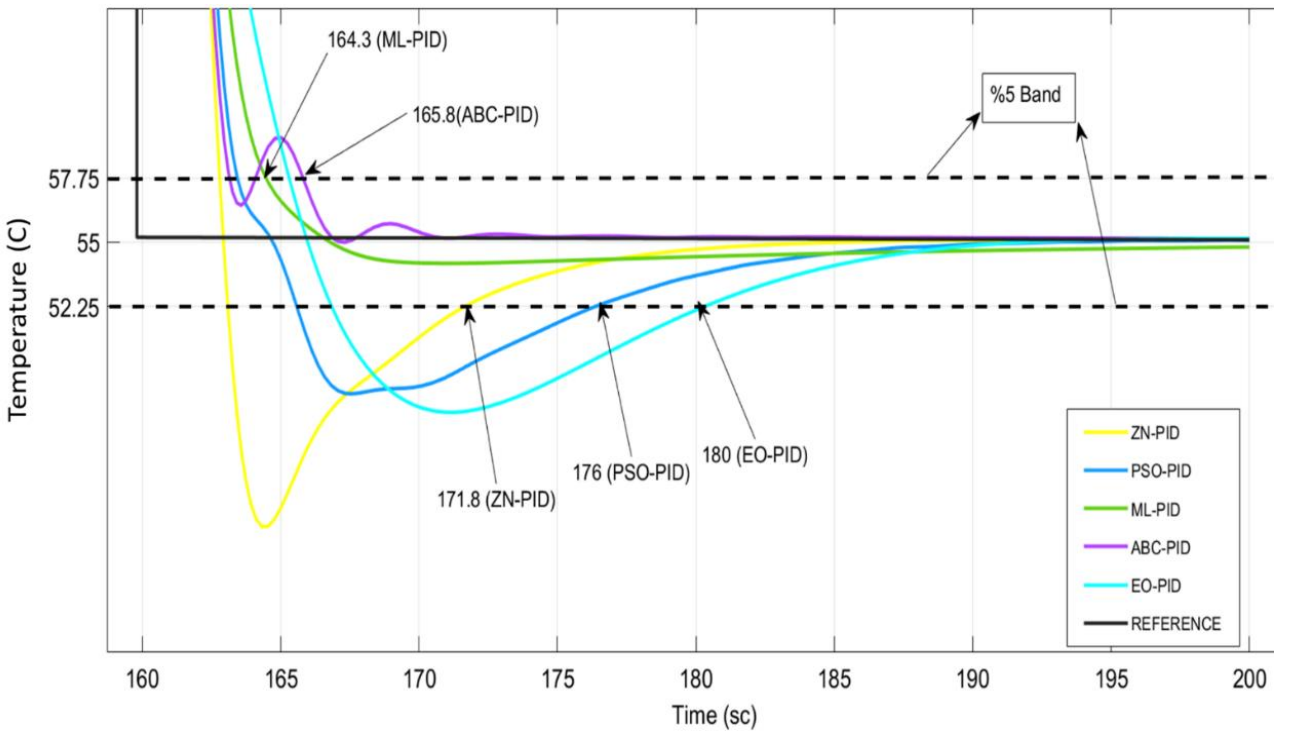


FIGURE 19. **Output signals of the TEC system between 160-200 seconds.**

Table 6 shows the settling times and maximum overshoot percentages for various time periods.

This work is licensed under a Creative Commons Attribution 4.0 License. For more information, see https://creativecommons.org/licenses/by/4.0/

This article has been accepted for publication in IEEE Access. This is the author's version which has not been fully edited and content may change prior to final publication. Citation information: DOI 10.1109/ACCESS.2024.3392734

TABLE 6: Transient regime criteria found from simulations.

Transient regime criteria		ML-PID	EO-PID	PSO-PID	ABC-PID	ZN-PID
0-40 Seconds	Settling Time (Sec)	4.86	22.24	18.63	6.14	13.48
	Overshoot (%)	3.01	17.8	16.8	9.47	30.5
40-80 Seconds	Settling Time (Sec)	44	61.2	57	45	52
	Overshoot (%)	1.27	13.8	12.1	6.72	22.5
80-120 Seconds	Settling Time (Sec)	83.4	84.25	82.8	82.8	86
	Overshoot (%)	0.5	4.6	4.4	2.4	6
120-160 Seconds	Settling Time (Sec)	123	124	122	122	126
	Overshoot (%)	0.6	4.01	3.15	2.2	6.31
160-200 Seconds	Settling Time (Sec)	162.5	178	172.9	165.2	170
	Overshoot (%)	0.6	9.09	7.27	7.74	20

When Table 6 is analyzed, it is observed that ML-PID gives better results in terms of settling time and overshoot percentage in both two regions (0-40 seconds and 40-80 seconds regions) compared to the others. When between 80-120 seconds region are examined, it is seen that PSO-PID and ABC-PID have the least settling time value as 82.8 second. However, ML-PID has the second lowest settling time, close to PSO-PID and ABC-PID. In addition, ML-PID have the least overshoot value (0.5%). Similarly, by examining the region between 120-160 seconds, it is seen that output signals for the micro-TEC system with PID controllers, which are optimized with PSO and ABC algorithms, have the least settling time value of 122 seconds. The signal with the least overshoot value (0.6 %) is reached when the ML method is used. ML-PID gives better results in terms of settling time and overshoot percentage in 160-200 seconds region compared to the others. When the results are evaluated in general, it can be seen that the ML-PID controller proposed in this study is much more successful than other controllers.

VII. CONCLUSION

In comparison with previous studies, our work proposes a unique approach by using the XGBoost algorithm and the generalized Hermite-Biehler theorem to calculate novel PID controller parameters that would enable robustly stable and optimal operation of the micro-TEC system in a PCR device. For the first time, XGBoost Hyperparameters with GridSearchCV were used to predict the PID controller parameters.

Machine learning method (ML-PID) and metaheuristic optimization algorithms, EO-PID, PSO-PID, and ABC-PID have been applied to our mico-TEC model and the results were compared in terms of settling time, the error and overshoot percentages. For each of the five PCR cycles, the micro-TEC with ML-PID controller was observed to settle for 4.86, 44, 83.4, 123, and 162.5 seconds, respectively, and overshoot values of less than 5%. The error percentages of ML-PID, EO-PID, PSO-PID and ABC-PID were calculated as 0.4%, 1.1%, 3.7% and 11.1%, respectively**.** In predicting the PID controller's parameters, the XGBoost algorithm obtained 91% test success and 97% training success. From the simulation results, it has been shown that ML-PID controllers applied in our micro-TEC system are compatible with the changing system conditions and contribute positively to the efficiency.

This work is licensed under a Creative Commons Attribution 4.0 License. For more information, see https://creativecommons.org/licenses/by/4.0/

This article has been accepted for publication in IEEE Access. This is the author's version which has not been fully edited and
content may change prior to final publication. Citation information: DOI 10.1109/ACCESS.2024.3392734

REFERENCES

1. K.B Mullis, F. Ferre, R.A. and Gibbs, The Polymerase Chain Reaction, Birkhäuser: Boston, USA, 1994.
2. A. Garg, U. Ghoshal, S. S. Patel, D. V. Singh, A. K. Arya, S. Vasanth, A. Pandey and N. Srivastava, "Evaluation of seven commercial RT-PCR kits for COVID-19 testing in pooled clinical specimens," Journal of Medical Virology, vol. 93, pp. 2281–2286, 2020,DOI: 10.1002/jmv.2669.
3. Z. Hanliang, Z. Haoqing, X. Ying, L. Sona, M. Korabecna, P. Neuzil, "Review PCR Past, Present and Future, BioTechniques," vol. 69, no. 4, pp. 317-325, 2020, DOI:10.2144/btn-2020-0057.
4. Khandpur, R. S.; Thermocycler (PCR Machine). Compendium of Biomedical Instrumentation. 2020, vol. 3, pp. 1927-1931, Wiley, DOI:10.1002/9781119288190.ch366.
5. Chen, J. J.; Hsieh I. H. Using an IR lamp to perform DNA amplifications on an oscillatory thermocycler. Applied Thermal Engineering. 2016, vol. 106, pp. 1-12, DOI:10.1016/ j.applthermaleng. 2016.05.184.
6. Y.F. Hsieh, E. Yoneza, L.S. Kuo, S.H. Yeh, P. J. Chen and P.H. Chen, "Polymerase chain reaction with phase change as intrinsic thermal control". Applied Physics Letters, vol. 102, no. 17, 2013, DOI: 10.1063/1.4803442.
7. W. Di, and Wenming, W. Battery powered portable thermal cycler for continuous-flow polymerase chain reaction diagnosis by single thermostatic thermoelectric cooler and open-loop controller. 2019, Sensors, MDPI, vol. 19, no. 1609, DOI:10.3390/s19071609.
8. J. Li, S. Liu, S. li, P. Zhang, H. Liu and L. Shao, "PCR Instrument Temperature Control System Based on Multimodal control," 2020 Chinese Control And Decision Conference (CCDC), Hefei, China, 2020, pp. 149-154, doi: 10.1109/CCDC49329.2020.9164539.
9. L. Xiao, Z. Wang, Z. Yu, H. Wu, Z. Zhang, Z. Ning and Y. Yu, "Multi-mode fuzzy control strategy of PCR precision temperature control system," The 2nd International Conference on Computing and Data Science (CONF-CDS 2021), January 2021, no. 129, pp. 1–7, Stanford, CA, USA, DOI:10.1145/3448734.3450859.
10. B. Liu L. Guo, Y. Deng, B. Zhang and N. He "Research of temperature control algorithm in PCR gene amplify instrument," IEEE International Symposium on Bioelectronics and Bioinformations, 03-05 November 2011, pp. 119-122, DOI: 10.1109/ ISBB.2011.6107660.
11. X. Qiu and J. Yuan, "Temperature control for PCR thermocyclers based on peltier-effect thermoelectric," Proceedings of the 2005 IEEE Engineering in Medicine and Biology 27th Annual Conference, September 1-4, 2005, pp:7509-7512, Shanghai, China, DOI: 10.1109/ IEMBS.2005.1616249.
12. A.-X. Pan, Zhao, W.; Zhang, M. Temperature-control algorithm design of the PCR instrument. 4th International Conference on Wireless Communications, Networking and Mobile Computing, pp.1-6, 12-14 October 2008, DOI: 10.1109/WiCom.2008.1210.
13. Y.K. Singh, J. Kumar, K.K. Pandey, K. Rohit and A. Bhargav "Temperature control system and its control using PID controller," International Journal of Engineering Research & Technology, CMRAES-2016, vol.4, issue. 2, pp. 1-3, Conference Proceedings, DOI: 10.17577/IJERTCONV4IS02010.
14. L. Li, L. Zhu, Q. Jiang and G. Liu, "Optimizing of thermal cycler control in microfluidic PCR system," Applied Mechanics and Materials, vol. 263- 266 (Part 1), pp. 713-717,2013.
15. M. P. Dinca, M. Gheorghe and P. Galvin, "Design of a PID Controller for a PCR Micro Reactor," in IEEE Transactions on Education, vol. 52, no. 1, pp. 116-125, Feb. 2009, doi: 10.1109/TE.2008.919811.
16. H.E. Kim, A. Schuck, WY. Kim, E.K. Jung, Y.H. Hong andY.S Kim, "PID temperature control system-based microfluidic PCR chip for genetic analysis," Journal of Electrical Engineering & Technology, vol. 17, pp. 495–501, 2022, DOİ:10.1007/s42835-021-00969-1.
17. T. Kadja, C. Liu ,Y. Sun, , V.P. Chodavarapu, "Low-cost, real-time polymerase chain reaction system for point-of-care medi cal diagnosis," Sensors, 22, 2320, pp. 1-14, 2022, DOI: 10.3390/ s22062320.
18. R. Khnouf, M. A. K. Jaradat, D. Karasneh, F. Al-Shami, L. Sawaqed and B. A. Albiss, "Simulation and Optimization of a Single Heater Convective PCR Chip and Its Controller for Fast Salmonella Enteritidis Detection," in IEEE Sensors Journal, vol. 20, no. 22, pp. 13186-13195, 15 Nov.15, 2020, doi: 10.1109/JSEN.2020.3004285.
19. H. Liu, Y. Fang, X. Su, Y. Wang, M. Ji, H. Xing, Y. Gao, Y. Zhang and N. He "Temperature control algorithm for polymerase chain reaction (PCR) instrumentation based upon improved hybrid fuzzy proportional integral derivative (PID) control," Instrumentation Science & Technology, 51:2, 109-131, 2023 DOI: 10.1080/10739149.2022.2105866.
20. S. Jun, Z. Meixia L. Zhengming and W. Xiaohong, "Simulation of Smith fuzzy PID temperature control in enzymatic detection of pesticide residues," Int J Agric & Biol Eng, , vol. 8, no.1, pp. 50-56, 2015.
21. S. Huang, J. Wu, H. Dai, R. Gao, H. Lin, D. Zhang, S. Ge, "Development of amplification system for point-of-care test of nucleic acid. Computer Methods in Biomechanics and Biomedical Engineering," vol. 25, no. 9, pp. 961-970, 2022, DOI: 10.1080/ 10255842.2021.1914022.
22. G.A. Nasser, A.L. Abdel-Mawgood, A.A. Abouelsoud, H. Mohamed, S. Umezu and A.M.R.F. El-Bab, 1New cost effective design of PCR heating cycler system using peltier plate without the conventional heating block," Journal of Mechanical Science and Technology. vol. 35, no.7, pp. 3259–3268, 2021, DOI:10.1007/ s12206-021-0646-5.
23. J. Shan, G. Wu and X Tian, "Study on large time-delay constant temperature control system based on TEC," The Journal of China Universities of Posts and Telecommunications. vol. 17, supplement. 2, pp. 32-35, 2010,DOI:10.1016/S1005-8885(09)60586-0.
24. S. Zhang, Y. Liu, M. Cheng and X. Zhao, "The fuzzy neural network temperature control in PCR reactor," Wireless Communications, Networking and Mobile Computing (WiCOM '08), October 2008. 4th International Conference, pp. 1-4.
25. L. Jun, W. Liu and T. Wang "Research and realization of algorithms for gene-chip PCR temperature-tracking control," Electronic Measurement & Instruments, 9th International Conference (ICEMI '09), August 2009, pp. 946-949.
26. S. Ekinci, D. İzci, L. Abualigah and R.A. Zitar, "A modified oppositional chaotic local search strategy based aquila optimizer to design an effective controller for vehicle cruise control system," Journal of Bionic Engineering, February 2023, DOI:10.1007/s42235-023-00336-y.
27. S. Ekinci, D. İzci and L. Abualigah "An effective control design approach based on novel enhanced aquila optimizer for automatic voltage regulator," Artificial Intelligence Review. vol.56, pp.1731–1762, 2023, DOI: 10.1007/s10462-022-10216-2.
28. R. Tabakh and H. Tiryaki, Control of the Automatic Voltage Regulator System with a Novel Stability-based Artificial Intelligence Method. Elektronika Ir Elektrotechnika, 27(6), 11-16, 2021, https://doi.org/10.5755/j02.eie.30143
29. V. Snásel, , R.M. Rizk-Allah, D. İzci and S. Ekinci, "Weighted mean of vectors optimization algorithm and its application in designing the power system stabilizer," Applied Soft Computing., vol.36, March 2023, DOI: 10.1016/j.asoc.2023.110085.
30. G. J. Silva, A. Datta and S. P. Bhattacharyya, "Controller design via Pade approximation can lead to instability," Proceedings of the 40th IEEE Conference on Decision and Control (Cat. No.01CH37228), vol. 5, pp. 4733-4737, 2001, DOI: 10.1109/CDC.2001.980953.
31. G. J. Silva, A. Datta and S. P. Bhattacharyya, "PID controllers for time-delay systems". Birkhäuser. 2005, ISBN: 0-8176-4266-8.
32. G. J. Silva, A. Datta and S. P. Bhattacharyya, "New results on the synthesis of PID controllers. IEEE Transactions on Automatic Control. 2002, vol.47, issue.2, pp. 241-252, DOI: 10.1109/9.983352.
33. G. J. Silva, A. Datta and S. P. Bhattacharyya, "Stabilization of first-order systems with time delay using the PID controller," Proceedings of the American Control Conference. 25-27 June 2001, pp:4650-4655, USA, DOI: 10.1109/ACC.2001.945713.

This work is licensed under a Creative Commons Attribution 4.0 License. For more information, see https://creativecommons.org/licenses/by/4.0/

This article has been accepted for publication in IEEE Access. This is the author's version which has not been fully edited and content may change prior to final publication. Citation information: DOI 10.1109/ACCESS.2024.3392734

34. Pontryagin, L. S. On the Zeros of Some Elementary Transcendental Function," American Mathematical Society Translation, 1955, vol. 2, pp. 95-110, 1955.
35. X. Zheng, X. Yu, X. Yang and W. X. Zheng, "Adaptive NN Zeta-Backstepping Control With Its Application to a Quadrotor Hover," in IEEE Transactions on Circuits and Systems II: Express Briefs, vol. 71, no. 2, pp. 747-751, Feb. 2024, doi: 10.1109/TCSII.2023.3309335.
36. X. Zheng, X. Yu, J. Jiang and X. Yang, "Practical Finite-Time Command Filtered Backstepping With its Application to DC Motor Control Systems," in IEEE Transactions on Industrial Electronics, vol. 71, no. 3, pp. 2955-2964, March 2024, doi: 10.1109/TIE.2023.3269478.
37. A. Yusuf, T. Koç, Y. S. Arıkuşu, H. Tiryaki, N. Bayhan and S. Ballikaya, "Modeling of a Thermoelectric Cooler System, Design and Optimization of the System's Controller," Sadhana, vol.47, no.182, pp. 1-530 August 2022, https://doi.org/10.1007/s12046-022-01954-8.
38. C. Wade, Hands-o-On Dradient Boosting with XGBoost and Scikit-learn, Packt, 2020.
39. A. Faramarzi, M. Heidarinejad, B. Stephens, S. Mirjalili, "Equilibrium optimizer: a novel optimization algorithm knowledge-based system," vol. 191, 105190, 2019, DOI: 10.1016/ j.knosys.2019.105190
40. J. Kennedy and R. Eberhart, "Particle swarm optimization," Proceedings of ICNN'95 - International Conference on Neural Networks, Perth, WA, Australia, 1995, pp. 1942-1948 vol.4, doi: 10.1109/ICNN.1995.488968.
41. D. Karaboğa, "An Idea Based on Honey Bee Swarm for Numerical Optimization," Technical Report TR06 Erciyes University Engineering Facultyvol. 200, pp. 1-10, 2005.
42. L. Ljung, Matlab User's Guide. 1, 237 (2011).
43. L. Ljung, R. Singh, Q. Zhang and P. Lindskog A. Iouditski, Developments in The MathWorks System Identification Toolbox, IFAC Proceedings, vol. 42(10) pp. 522-527, 2009.
44. J.G. Ziegler, N.B. Nichols and N.Y. Rochester Optimum settigs for automatic controllers. Transactions of the American Society of Mechanical Engineers. 1942, vol. 64, pp. 759-768.
45. A. Géron, "Hands-On Machine Learning with Scikit-Learn, Keras, and TensorFlow: Concepts, Tools, and Techniques to Build Intelligent Systems," 2019.
46. A. C. Kelle and H. Yüce, "MQTT Trafiğinde DoS Saldırılarının Makine Öğrenmesi ile Sınıflandırılması ve Modelin SHAP ile Yorumlanması". Journal of Materials and Mechatronics: A (JournalMM), 3(1), 50-62. 2022 (In English: A. C. Kelle, H. Yüce, "Classification of DoS Attacks in MQTT Network with Machine Learning and Interpretation of The Model with SHAP," Journal of Materials and Mechatronics: A (JournalMM), 3(1), 50-62,2022.



Yılmaz Seryar ARIKUŞU was born in Mersin in 1992. He received his B.Sc degree in Electrical and Electronic Engineering from Isık University in 2015. He completed his M.Sc. degree in Electrical and Electronics Engineering from Istanbul Bilgi University in 2018. He is currently research assistant the Electrical Engineering Department of Manisa Celal Bayar University. He is also Ph.D candidate in Electrical and Electronics Engineering at Istanbul University-Cerrahpasa. He is member of IEEE student. His research interests are automatic control systems, hybrid electric vehicles, artificial intelligence, robust control, control system design, metaheurisctic optimization algorithms.



Nevra BAYHAN was born in Istanbul. She received her B.Sc. degree (Hons.) and M.Sc. degree in Electrical and Electronics Engineering from Istanbul University in 1997 and 2001, respectively. She completed her Ph.D. in Control and Automation Engineering at Istanbul Technical University in 2008. She is currently an assist Professor at the Electrical and Electronics Engineering Department of Istanbul University-Cerrahpasa. From 2017 to 2022, she has worked as the Head of Main Scientific Branch Control and Command Systems of Electrical and Electronics Engineering Department, Istanbul University-Cerrahpasa. Her research interests include automatic control systems, control systems design, artificial intelligence, metaheurisctic optimization algorithms, time-delay systems, heat transfer in thermoelectric power generation (TEG) and thermoelectric cooling (TEC) systems, system modeling, fuzzy control, low order controller design, renewable energy systems, robust control, digital control systems, hybrid electric vehicles and control of systems with parameter uncertainties.

This work is licensed under a Creative Commons Attribution 4.0 License. For more information, see https://creativecommons.org/licenses/by/4.0/